Review and perspectives from researchers led by Dr. Stuart R. Miller, a fellow of the Royal Society of Chemistry, at the Materials Discovery Research Institute, UL Research Institutes, Skokie, Illinois, USA.

High throughput computational and experimental methods for accelerated electrochemical materials discovery

The Materials Discovery Research Institute (MDRI) at UL Research Institutes is dedicated to pioneering new materials that aspire to solve pressing global safety challenges. By harnessing the power of advanced computing and high-throughput experimental methods, we are creating groundbreaking materials that support renewable energy and environmental sustainability, all while ensuring a mindful approach to human health.

Image reproduced by permission of UL Research Institutes, *J. Mater. Chem. A,* 2025, **13**, 26041.

As featured in:

See Stuart Miller, Jinfeng Wu *et al.*, *J. Mater. Chem. A,* 2025, **13**, 26041.

ROYAL SOCIETY OF CHEMISTRY

rsc.li/materials-a

Registered charity number: 207890

Journal of Materials Chemistry A

ROYAL SOCIETY OF CHEMISTRY

REVIEW

View Article Online
View Journal | View Issue

Cite this: J. Mater. Chem. A, 2025, 13, 26041

High throughput computational and experimental methods for accelerated electrochemical materials discovery†

Uzoma Nwabara, Kunran Yang, Akshay Talekar, Varinia Bernales, Jorge González, Stuart Miller * and Jinfeng Wu *

The full integration of sustainable technologies to combat climate change heavily depends on the discovery of cost-competitive, safe, and durable performative materials, specifically for electrochemical systems that can generate energy, store energy, and produce chemicals. Due to the vast exploration space, scientists have adapted high throughput methods, both computational and experimental, for screening, synthesis, and testing to accelerate material discovery. In this review, we analyze such high throughput methodologies reported in the literature that have been applied to electrochemical material discovery. We find that most reported studies utilize computational methods, including density functional theory and machine learning, over experimental methods. Some labs have combined computational and experimental methods to create powerful tools for a closed loop material discovery process through automated setups and machine learning. Either way, over 80% of the publications we reviewed focus on catalytic materials, revealing a shortage in high throughput ionomer, membrane, electrolyte, and substrate material research. Moreover, we find that most material screening criteria do not consider cost, availability, and safety, all of which are crucial properties when assessing the economic feasibility of proposed materials. In addition, we discover that high throughput electrochemical material discovery research is only being conducted in a handful of countries, revealing the global opportunity to collaborate and share resources and data for further acceleration of material discovery. Finally, we acknowledge the development of autonomous labs and other initiatives as the future of high throughput research methodologies.

Received 13th January 2025
Accepted 14th July 2025

DOI: 10.1039/d5ta00331h

rsc.li/materials-a

1. Introduction

Rising atmospheric and oceanic levels of CO_2 and other greenhouse gases have been associated with an increase in the average global temperature.[1,2] This phenomenon negatively impacts Earth's ecosystems, and we have already seen proof through extreme weather and temperature anomalies worldwide. Growing demand for energy, food, and other resources goes hand in hand with population growth in various developing countries.[3,4] Such demands contribute to our output of these harmful gases, especially if we continue our current practices to meet them.[5,6] Scientists around the world have proposed and researched a plethora of technologies to reduce CO_2 emissions or mitigate the existing atmospheric and oceanic CO_2 concentrations. Some of these technologies include nuclear, wind, and solar energies, direct air capture, large-scale batteries for excess energy storage and powering vehicles, hydrogen fuel cells, water splitting, and electrochemical CO_2 reduction to name a few.[7,8]

The accelerating climate crisis and rising energy demands require sustainable electrochemical technologies for energy storage, generation, and chemical production. Over the past two decades, electrochemical technologies have gained much attention due to improved material and reactor performance and new material discovery, propelling commercialization and scale-up. However, key performance benchmarks (*e.g.*, activity, selectivity, and energy efficiency) still need to be achieved before such emerging technologies can compete economically with existing fossil fuel-based processes.[9–13] Material bottlenecks—such as cost, durability, and scalability, continue to limit progress. For example, precious metal catalysts such as platinum, gold, and iridium are still state of the art for many electrochemical reactions. At the same time, the substrates, ionomers, membranes, and electrolytes used in the reactors degrade over long-term operation, posing significant challenges. Additionally, safety concerns must be considered when scaling up the production and handling of such materials. Overcoming these barriers requires discovering and

Materials Discovery Research Institute, UL Research Institutes, Skokie, Illinois, 60077, USA. E-mail: stuart.miller@ul.org; jeff.wu@ul.org

† Electronic supplementary information (ESI) available. See DOI: https://doi.org/10.1039/d5ta00331h

introducing new materials and methods that are more cost-effective, stable, and safer to drive feasibility.

In recent decades, many researchers have successfully identified, synthesized, and characterized promising materials through standard benchtop chemistries and instruments. Yet, the conventional approach in these studies involves proposing, synthesizing, and testing one material, meaning that the research and discovery timescale for each material can take months or even years. Despite the multitude of groups across the globe committed to developing electrochemical technologies, this rate of material discovery is simply not sufficient, as we have yet to reach the needed benchmarks for feasibility. High-throughput (HT) computational and experimental methods offer a transformative solution by significantly accelerating material discovery to meet these global challenges.[14–17] Here, HT methods involve setups or techniques designed for fully synthesizing, characterizing, screening, or analyzing multiple materials samples in a shorter time than traditional benchtop chemistry and engineering.

Unsurprisingly, the advancement and availability of theoretical prediction methods and supercomputing in the last 20–30 years have encouraged the use of simulated chemistry experiments. These simulations not only predict and explain material performance but also suggest new materials for synthesis and testing. Reported computational chemistry studies in the literature depict the ability to explore and screen materials in the order of 10^6 in a single project using methods such as first-principles density functional theory (DFT) and advanced machine learning (ML) techniques, including deep learning and active learning (AL). Moreover, HT experimentation has expanded with new setups created to test or characterize tens or hundreds of samples in days instead of months or years. As shown in Fig. 1, the integration between computational and experimental HT approaches is also promising and imperative for fast-tracking material discovery, which will help progress sustainable electrochemical technologies. Other researchers have stressed the need for experimental validation in HT computational screening workflows as well.[18]

By screening millions of material candidates computationally and validating the most promising experimentally, high-throughput workflows drastically reduce discovery timelines. This acceleration is critical for achieving key performance benchmarks required for the commercialization of renewable technologies, such as green hydrogen production, carbon capture, and advanced energy storage. Here, we review high-throughput methods—both computational and experimental—from the literature dedicated to discovering materials (catalysts, electrolytes, ionomers, *etc.*) for electrochemical energy applications. The objective of this review is to provide an overview of the popular HT techniques, state-of-the-art materials, and novel setups to serve as a reference point for scientists currently incorporating or initiating HT approaches into their research. We first highlight notable efforts with exceptional performance or unique setups, as well as common focuses and approaches. Finally, we provide an overview and a perspective of gaps that are worth further exploration.

2. Computational methods

Over the past few decades, the utilization of computational methods for material discovery has typically been driven by three major goals: (i) providing a deep understanding of the structure and structural dynamics of materials, as well as their relationship with properties and catalytic activity, (ii) unraveling

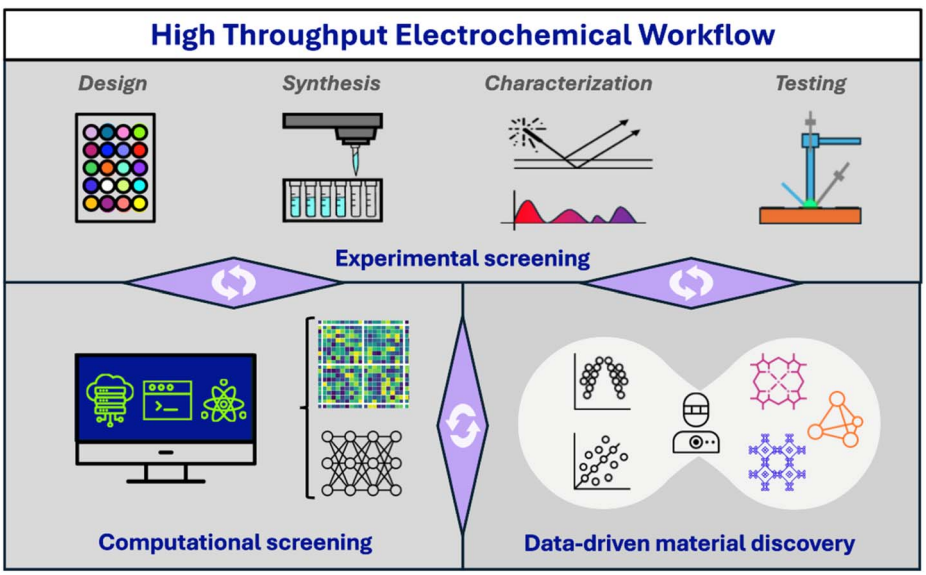

Fig. 1 Schematic of high-throughput platforms for electrochemical materials discovery: an iterative feedback loop between experimental and computational methods to enhance accuracy and speed in material selection and optimization. This figure presents the general workflow framework. The challenges and experimental/computational considerations are addressed in detail in the accompanying methodology sections and case studies of this review.

the underlying structure–function relationships to facilitate the discovery of novel materials, and (iii) enabling exploration of large chemical spaces to predict materials with superior properties.[19,20] These goals can be achieved using a variety of methods, including quantum mechanical calculations, atomistic simulations, and materials informatics. Nowadays, we can tackle more complex systems that encompass multiple components; however, modeling multiple experimental parameters and processes that accompany the development of these materials poses a great challenge for virtual material screening. HT computational methodologies can effectively undertake such multifactorial problems. Yet two of the most significant drawbacks of HT computational screening are (i) developing a robust, effective, and efficient HT workflow and associated databases and (ii) finding the balance between cost and accuracy when dealing with complex or large-scale systems.[21] This section reviews key methodologies and descriptors utilized in the HT computational studies examined herein, with a particular focus on DFT and ML, two of the most common approaches applied in HT material discovery campaigns in electrochemistry.

2.1 Common approaches

2.1.1 Density functional theory. Thanks to its relatively low computational cost and semiquantitative accuracy, DFT has been widely employed in materials science to predict properties based on the electronic structure.[22,23] DFT is rooted in quantum and statistical mechanics, relying on principles derived from these fields to find approximate solutions to the Schrödinger equation and determine the ground-state electronic density of a material.[24,25] Over time, DFT has provided deeper insight into materials' electronic structure, enabling the prediction of properties such as bandgaps, which are crucial for classifying new materials as metals, semiconductors or insulators. A critical factor when applying DFT is the choice of the density functional, which determines the accuracy and predictive power of the simulations.[22,26–29] While DFT is often employed to provide a static view of a system and characterize its intrinsic properties, it can also be applied to investigate dynamic behavior and the equilibrated structures under different conditions, such as temperature and pressure. In this regard, DFT can be used in conjunction with classical or *ab initio* molecular dynamics and Monte Carlo simulations but at the expense of higher computational costs.[30–33]

To further minimize the computational cost associated with these calculations and facilitate large-scale material screening, DFT has been extensively used to compute descriptors—quantifiable representations of specific properties that connect complex electronic structure calculations and macroscopic properties. An effective descriptor can serve as a valuable metric for identifying promising candidates.[34,35] A relevant example is the study of electrocatalysts, which are typically evaluated based on their reactivity toward a particular reaction. The reactivity descriptor that can quantify the catalyst's activity is often represented by the Gibbs free energy (ΔG) associated with the rate-limiting step (RLS) of the reaction. In many cases, the RLS is determined by the adsorption of one or one set of given reactants or intermediates. With this and the development of the computational hydrogen electrode model by Nørskov *et al.*,[36] adsorption energy has become a well-studied descriptor for predicting catalytic activity. While activity and selectivity are crucial metrics for a successful catalyst, other essential factors, including chemical and electrochemical stability, must be considered. A comprehensive list of commonly used descriptors is provided in Section 2.1.2 and Table 1, and a detailed description of the most common methodologies in computational HT is given in ESI Table S1.† While convergence thresholds are system-dependent and therefore not directly comparable across studies, readers are directed to the original literature for application-specific optimization details.

2.1.2 Commonly used descriptors. Generally, descriptors can be classified into five categories, namely thermodynamic, electronic, mechanical, geometric, and intrinsic structures. Thermodynamic descriptors are the most frequently used, relying on energetics to evaluate systems' behaviors; they often establish physical relationships with the target electrochemical property, are readily calculated, and can be a good start for quickly estimating energetic trends. Examples of such descriptors include adsorption energies and theoretical overpotential terms. These descriptors can also assess competing reactions and their mechanisms. For instance, the adsorption-free energy of the H atom (ΔG_H) can describe activity towards the hydrogen evolution reaction (HER), while ΔG_{CO}, ΔG_{CHO}, and ΔG_{OH} correlate with the electrochemical reduction of CO_2 (eCO_2RR).[37] The selectivity between these reactions can be evaluated by comparing the critical ΔG_s of the HER and eCO_2RR. Additionally, thermodynamic descriptors can reflect structural stability under electrochemical conditions, including properties such as surface energy, formation energy, segregation energy, decomposition energies,[57,66,67,78,79] dissolution potential[44,60,63,78,80] and Pourbaix diagrams.[60,78]

The second prominent descriptor type involves the electronic structure aspect and its derived properties, *e.g.*, the d-band center, band gaps, work functions, phonon spectra, metal-induced electronic states, and charge variations. These descriptors are typically obtained from DFT-level calculations, unveiling atomic interaction and electronic features. However, due to the complex impact of electronic structures on reactivity and materials' properties, these descriptors may not indicate the same trend when conducting structure prediction for different systems. Mechanical descriptors, including elastic constants, Young's modulus, and glass transition temperature, are frequently reported in the literature, as they are used for predicting and comparing experimentally measurable properties. Geometric descriptors are similarly valuable and can vary based on material types. Examples include the rotation angle of heterojunctions, the distance contribution descriptor, the transition metal–oxygen bond length for mixed metal salts, and the coordination number in alloys, among others.[46,50] These descriptors are often directly calculated through structural optimization, and no further electrochemical studies are needed. Therefore, they are efficient in predicting the structures' properties when there is a clear structure–property

Table 1 Summary of computational methods, models, algorithms and descriptors utilized for HT screening of catalysts, ionomers and electrolytes. Most studies suggest materials to consider for experimental screening based on their computation results. DFT indicates density functional theory, while ML indicates machine learning. All acronyms not previously mentioned in the text are defined in table footnotes[a]

		Method(s)							
Material	Rxn(s)	DFT	ML	Descriptor(s)	ML algorithm		Suggested material(s)		Year	Ref.
Catalyst	eCO_2RR	✓	✓	ΔG_{CO} ΔG_{CHO} ΔG_{OH} Limiting potential differences	ETR SVM GBR	GPR KRR XGB	CrN TiN Cr_3N_2 Cr_2N CoN		2023	37
Catalyst	eCO_2RR	✓	✓	ΔG_{CO}	ANN		None stated		2015	38
Catalyst	eCO_2RR	✓		ΔG_{CO} $\Delta G_{OOH/CHO}$	N/A		N_6V_4–AgCr		2021	39
Catalyst	eCO_2RR	✓		ΔG_{CO} ΔG_{OH}	N/A		None stated		2020	40
Catalyst	HER	✓		ΔG_H	N/A		NbS_2 Ba_2Cu_2 C_8 $Pr_4C_2Cl_5$ $Ce_4C_2Br_5$	$IrTe_2$ $NbSe_2$ Ti_2Se_2 $TaSe_2$	2020	41
Catalyst	HER	✓	✓	Zero band gap Thermodynamic stability Low vacancy formation energy ΔG_H	LSR GBR RFR ANN		VS_2 NiS_2 $ZrTe_2$ PdTe	MnS_2 $CrSe_2$ $TiTe_2$ VSe_2	2021	42
Catalyst	HER	✓	✓		RNN KRR	SVM RF	OsB_2 Sc–N		2020	43
Catalyst	HER	✓	✓	Thermodynamic stability energy Dissolution potential ΔG_H	AB CBC RNC LR HGB Bagging LGBM	GBR XRT RF DT SVM KNN XGB	$Pd@B_4$ $Ru@N_2C_2$ $Pt@B_2N_2$ $Fe@N_3$	$Fe@P_3$ $Mn@P_4$ $Fe@P_4$	2022	44
Catalyst	HER	✓		ΔG_H	N/A		$Zn@MoS_{va}Se$ $Cd@MoS_{va}Se$ $Co@Mo_{va}SSe$		2021	45
Catalyst	HER	✓	✓	Rotation angle of heterojunctions	LAS		$MoTe_2/WTe_2$		2020	46
Catalyst	HER	✓		Number of valence e^- × electronegativity of dopants ΔG_H	N/A		None stated		2022	47
Catalyst	HER	✓		Strain energy (includes ΔG_H, exchange current, overpotential, and TOF)	N/A		Fe–N-SWCNTs		2023	48
Catalyst	HER	✓	✓	"Frozen" ΔG_H Relaxation energy	ANN	GBDT	None stated		2020	49
Catalyst	HER	✓	✓	Distance contribution descriptor	SVM		$Pt_{33}Pd_{17}Ni_{15.5}Cu_{16}P_{18.5}$		2023	50

Table 1 (*Contd.*)

Material	Rxn(s)	Method(s) DFT	Method(s) ML	Descriptor(s)	ML algorithm		Suggested material(s)		Year	Ref.
Catalyst	HER	✓	✓	Variety (22)	RF AB KNN KRR PLS	LSR RDG GBR MLP SVM	CN/MX_2 heterostructures w/Sc and Ti intercalated		2024	51
Catalyst	HER	✓	✓	ΔG_H	AB ENR GBR KNN KRR	LAS PLS RF RDG	28 promising materials in SI		2023	52
Catalyst	HER	✓	✓	ΔG_H Cohesive energy	RF ANN SVM LAS KNN Bayesian		$Ti_3C_2I_2$–Ir $Ti_3C_2Br_2$–Cu $Ti_3C_2Br_2$–Pt $Ti_3C_2Cl_2$–Cu $Ti_3C_2Cl_2$–Pt $Ti_3C_2Se_2$–Au $Ti_3C_2Te_2$–Nb		2022	53
Catalyst	HER NORR	✓		Adsorption energy Limiting potential Ratio of the d-band center + ratio of the work function	N/A		Co–pyromellitic dithioanhydride (HER) Co–3,8-phenanthroline-5,6-dione (NORR) Co–phenan-thraquinone (NORR)		2023	54
Catalyst	HER ORR	✓	✓	ΔG_{CO} ΔG_H ΔG_O	GNN		Cu_3Pt $FeCuPt_2$		2021	55
Catalyst	HER OER	✓	✓	ΔG_H ΔQ_{Cu-Cu}	ANN		None stated		2021	56
Catalyst	NRR	✓	✓	Segregation energy ΔG_N	RF		Zr_1Cr Hf_1Cr		2024	57
Catalyst	NRR	✓	✓	Isolated electron number of d orbitals	BRT		Mo and W		2021	58
Catalyst	NRR	✓		Binding energy between metal atoms Cohesive energy ΔG_N Limiting potential	N/A		Mo@BM-β_{12} Mn@BM-β_{12}		2021	59
Catalyst	OER	✓		Pourbaix (Nernst eqn) ΔG_O ΔG_{OH}	N/A		Co–Ir Fe–Ir Mo–Ir		2020	60
Catalyst	OER	✓	✓	Transition metal–oxygen bond length First ionization energy	GBR		IrO_2 $Fe(SbO_3)_2$ $Co(SbO_3)_2$ $Ni(SbO_3)_2$ $FeSbO_4$	$Fe(SbO_3)_4$ $MoWO_6$ $TiSnO_4$ $CoSbO_4$ $Ti(WO_4)_2$	2024	61
Catalyst	OER ORR		✓	Area-specific resistance	RF		$SrZr_{0.125}Nb_{0.125}Co_{0.625}Cu_{0.125}O_3$ $K_{0.25}Sm_{0.125}Sr_{0.625}Nb_{0.125}Ta_{0.125}Co_{0.75}O_3$ $Bi_{0.125}Sr_{0.875}Y_{0.125}Ni_{0.125}Co_{0.75}O_3$		2024	62

Table 1 (*Contd.*)

Material	Rxn(s)	Method(s) DFT	Method(s) ML	Descriptor(s)	ML algorithm	Suggested material(s)	Year	Ref.
Catalyst	OER ORR	✓		Cohesive energy ΔG_x Elastic constants Phonon distribution Formation energy Dissolution potential	N/A	IrN_2 monolayer	2021	63
Catalyst	OER ORR	✓	✓	ΔG_{OH} ΔG_{OOH} ΔG_O ΔG_{OOH} Coordination number 6 more features	XGB RF ETR GBR	None stated	2024	64
Catalyst	ORR		✓	Itinerant electrons	XGB LGBM ANN	15 different materials predicted	2024	65
Catalyst	ORR	✓		Surface energy Segregation energy d-Band center ΔG_O	N/A	Ag_3(Mn, Fe, or Co) Ag_3(Zr, Mo, or Ru) Ag_3(Ta and W) Ag–(Mn or Fe) Ag–(Ta or W)	2016	66
Catalyst	ORR	✓		Formation energy Single atom binding energy ΔG_{OH} ΔG_{OOH}	N/A	$Co–ON_3$	2022	67
Catalyst	ORR MOR	✓		Oxygen vacancy formation energy Single Pt atom adsorption energy Metal-induced electronic states Charge variation of deposited Pt	N/A	Dependent	2017	68
Ionomer	ORR		✓	Proton conductivity Water uptake Gas permeability Band gap Thermal decomposition temperature Glass transition temperature Young's modulus	GPR	60 new polymer candidates	2023	69
Electrolyte		✓		Adiabatic redox energy Vertical redox energy Reorganization energy	N/A	$LiNi_{0.5}Mn_{1.5}O_4$	2015	70
Electrolyte		✓		Stoichiometrically valid reactions	N/A	None stated	2023	71
Electrolyte		✓		Redox potential Solubility Stability	N/A	None stated	2015	72
Electrolyte		✓	✓	Trajectory	GNN	None stated	2023	73

Table 1 (*Contd.*)

Material	Rxn(s)	Method(s)		Descriptor(s)	ML algorithm	Suggested material(s)		Year	Ref.
		DFT	ML						
Electrolyte		MD	✓	Ionic conductivity	minGPT	None stated		2024	74
					1Ddiffusion				
					Diffusion-LM				
Electrolyte		MD	✓	Ionic conductivity	minGPT	None stated		2024	75
Electrolyte		✓	✓	Diffusion coefficient	BO	Li_3YBr_6		2025	76
Electrolyte			✓	Ion conductivity	GNN	Li_6PBrO_5	Li_2AsF_5	2024	77
					GBDT	$Li_2Ta_2O_3F_6$	$LiZnPSe_4$		
						$Li_{10}Mg_7Cl_{24}$	$LiHgPSe_4$		
						$Li_7Cl_3O_2$	$LiBSe_2$		
						Li_2SbF_5	$LiCuBr_2$		

[a] ETR: extra-trees regressor, SVM: support vector machine, KRR: kernel ridge regressor, XGB: extreme GBR, ANN: feedforward artificial NN, LSR: least squares regression, RNN: recurrent NN, CBC: CatBoost classifier, RNC: radius neighbors classifier, LR: logistic regression, HGB: histogram-based GBR, LGBM: light gradient boosting machine, XRT: extremely randomized trees, DTs: decision trees, KNN: *k*-nearest neighbors, LAS: lasso regression, GBDT: gradient boosting decision tree, AB: AdaBoost, PLS: partial least squares, RDG: ridge regression, MLP: multilayer perceptron, ENR: elastic net regressor, GNN: graph NN, NORR: NO reduction reaction, BRT: boosted-regression-tree, MOR: methanol oxidation reaction, MD: molecular dynamics, minGPT: minimal generative pretraining transformer, 1Ddiffusion: 1D denoising diffusion probabilistic model, Diffusion-LM: diffusion language model, and BO: Bayesian optimization.

relationship. Finally, the intrinsic-structure descriptors gather prior knowledge from either theories or experiments, and they often do not require DFT calculations. These descriptors vary by material type and their respective properties such as the number of valence electrons, dopant electronegativity, the number of isolated d-orbital electrons, and the first ionization energy. These properties have been well studied and reported, and hence these descriptors can be easily implemented in material screening workflows where the studied materials normally have well-defined structures. For HT studies and screening, many researchers use multiple descriptors or modify common descriptors to increase scrutiny and find more applicable materials.

2.1.3 Machine learning. ML models leverage mathematical relationships and statistical methods to generate predictions, often without directly incorporating specific chemical knowledge or theories. The training process involves feeding a model a dataset (the training dataset), enabling it to recognize patterns, trends, and relationships to then make predictions on new, unseen data (the testing dataset).[81] ML offers a diverse array of learning algorithms; the selection depends on several factors, such as the prediction task at hand, size and type of data, and data quality, to name a few. Access to different algorithms grants the choice of one that best suits the problem at hand and minimizes error (*e.g.*, root mean square error, RMSE) while considering factors such as model interpretability, complexity and computational efficiency.[81] Table 1 highlights several common ML algorithms employed in the computational HT studies examined in this review, which include neural networks (NNs), random forest regression (RFR), gradient boosting regression (GBR) and Gaussian processes regression (GPR). A more detailed table is available in the ESI.†

The integration of ML methods in HT material discovery processes has already showcased multiple advantages.[29] Different algorithms allow models to be trained on various data types (graph, numeric, image, natural language, *etc.*) and enable many different predictive tasks (regression, classification, data generation, *etc.*). Thus, ML can be applied to a myriad of use cases for materials discovery. For example, ML methods can predict material synthesizability by analyzing existing experimental data such as reaction conditions and time. In addition, ML models or their key features can also accelerate DFT calculation processes and reduce calculation workloads when searching a vast compositional space. This is often done by training ML models using DFT data. Additionally, multiple data sources (experimental, computational, literature, *etc.*) can be integrated into ML models, making HT experiments and calculations faster, more scalable, and more suitable for complex multifactor-dependent material systems. Another advantage ML methods offer is the ability to implicitly build relationships and patterns between independent and dependent variables, such as structural features (*e.g.*, composition) and macroscopic properties (*e.g.*, conductivity), respectively, within a dataset. Therefore, scientists can better understand materials and then exploit these relationships to drive innovation through inverse material design where ML models predict hypothetical structures with targeted properties. The versatility

of ML makes it a powerful tool for creating new solutions to computational materials discovery.

In recent years, the use of generative AI models (large language models, diffusion models, reinforcement learning-based generative models, *etc.*) in materials design has been on the rise. Yet, generative AI is still limited to applications in academia and research as evidence of its applications in industry or production/manufacturing environments is lacking. In research applications, scientists have applied generative AI to aid in materials discovery. For example, Song *et al.* and Li *et al.* applied inverse material design *via* ML to synthesize materials with specific properties for electrochemical CO_2 reduction or high-capacity energy storage, respectively.[82,83] Moreover, Alverson *et al.* utilized generative AI models such as variational auto-encoders, generative adversarial networks, and genetic algorithms as use cases for creating crystals and proposing new structures.[84] Additionally, Bang, Kim, Hong *et al.* expanded on inverse design using generative AI models to discover materials with multiple properties, rather than optimizing a single property.[85] While generative AI in materials discovery shows promise in limited applications in electrochemical materials discovery, it shares many of the pain points seen in other ML methods, such as a lack of publicly available robust training datasets and the limited ability of models to generalize outside of training dataset distributions and to real world experimentation.

While ML is a powerful tool that helps improve the quality and efficiency of the HT materials discovery process in many ways, it comes with drawbacks and challenges. First, insufficient high-quality data impede training accurate, generalizable machine learning models.[86] Data-intensive ML models such as NNs and RFR require large, information-dense datasets for suitable performance. Creating datasets from experimental work, especially when traversing all possibilities of a material database, is demanding as experiments are expensive and time-consuming, require highly skilled experts, and are often proprietary. A lack of quality data can lead to poor model predictions when exploring beyond a model's training dataset distributions. Second, integrating multiple data sources (such as experimental work and DFT simulations) to train ML models lacks standardization, making collaborative efforts to solve problems in the field more challenging.[87] Third, many ML algorithms behave as a "black box", making their predictions challenging to trust and their proposed structure–property relationships impossible to explain explicitly. Nevertheless, these challenges can be addressed by building more robust and interpretive models and placing an emphasis on standardizing data handling practices.[87]

2.1.4 Density functional theory *versus* machine learning. Both DFT and ML are useful methods for HT material screening and discovery. Yet, each has its own advantages that make one more suitable for certain applications than the other. For instance, DFT simulations tend to be computationally intensive especially when modelling complex systems and large unit cells, or exploring a large chemical search space, limiting their feasibility for large scale screening. However, ML models, once trained on reliable datasets, can enable rapid predictions of properties at a fraction of the cost. This ability to scale easily makes ML attractive for large scale screening tasks.

In contrast, the quality of ML models relies heavily on the amount and diversity of high-quality datasets, and their predictive ability often degrades when predicting beyond the distribution of the training sets. As a result, real-world applications of ML in HT discovery of materials require careful consideration when curating a training dataset and can be aided by uncertainty quantification and ongoing benchmarking against DFT calculations and real-world experiments.

A hybrid approach that combines DFT and ML leverages the complementary strengths of both methods to overcome their individual limitations. DFT calculations provide high-fidelity, physics-based training data with reliable energetics and electronic properties for well-defined material systems, serving as the foundation for accurate ML model development. Quantum chemical calculations ensure that the training dataset captures the fundamental physical relationships between structures and properties. Conversely, ML models trained on these high-quality DFT data can rapidly screen candidate materials at a larger scale with a fraction of the computational cost, enabling exploration of vast chemical spaces that would be prohibitively expensive using DFT alone. Readers are referred to Section 4 for examples of the combinatorial approaches.

2.1.5 Limitations and considerations in computational methods. While theoretical calculations have enabled significant advances in electrochemical materials discovery, several fundamental limitations affect their application in high-throughput screening.[88] First, accuracy-efficiency trade-offs are inherent to all computational methods. DFT functional selection significantly impacts results, with different functionals yielding distinct trends that can affect screening outcomes. Second, reaction condition complexity presents major challenges, as electrochemical processes involve multiple variables (electrolytes, pH, applied potentials, temperature, *etc.*) that are computationally expensive to model explicitly. Many studies rely on simplified models that may not capture realistic operating conditions, such as using DFT energies rather than free energies, which are unable to obtain energetics at experimental temperatures. Third, kinetic limitations are often overlooked, as most screening approaches use thermodynamic descriptors rather than kinetic parameters, potentially missing important rate-determining factors and complex reaction mechanisms. Finally, transferability issues arise when force fields or ML models trained on specific systems are applied to broader materials classes without adequate validation.

Data reproducibility remains a major bottleneck in computational materials discovery. Experiments from which training datasets are derived may have similar product compositions but differ in the structure or properties due to changes in process parameters. Reproducibility can be improved by thorough capture of metadata and tracking key information such as ingredient lots, sample storage conditions, equipment calibration logs, *etc.* Initiatives such as the Materials Genome Initiative, Materials Acceleration Platform, and, for computational datasets, Novel Materials Discovery aim to improve reproducibility by hosting datasets that have detailed metadata, thus

permitting multi-organizational validation of workflows.[89–91] Reproducibility is also aided by laboratory information management systems that can assist in capturing metadata, process parameters, and equipment information, which allow more systematic and comprehensive experimentation records. Traditional lab equipment with automated data logging capabilities (*e.g.*, ThermoFisher and HeiDolph) also helps reduce data noise and user input errors, which benefits experimental reproducibility. Automated chemistry platforms with end-to-end logging, such as Chemspeed and Unchained Labs automated platforms, are also helping to reduce human-caused variability to ensure reproducibility. Additionally, performing replicate analysis under controlled conditions will aid in improving reproducibility, allowing researchers to identify outliers. Replicate analysis must be balanced with resource limitations carefully as it is expensive and can be out of reach for many groups.

Standardized procedures enhance reproducibility as using agreed upon standards makes collaborative efforts and experimental validation simpler.[92] Inconsistencies in procedures for characterization, calibration, or sample storage demand correction through standardization. Adopting community standards for experimental work can help reduce noise within experimental datasets and improve reproducibility.

In addition to improving experimental data quality *via* noise reduction, researchers can use data curation and filtration techniques. For example, anomaly detection using statistical thresholds and certain ML techniques (*e.g.*, clustering or isolation forests) can reduce outliers from experimental data. Moreover, validating experimental data with computational results allows researchers to identify experiments that may have strayed from theoretical expectations. This technique could also be used to reduce the cost of replicate analysis as only samples that deviate from theoretical expectations would require such analysis.

Experiment reproducibility also affects ML, a data-driven technique. The usefulness of ML models depends on how well their predictions can generalize to physical experiments. Thus, if ML models are trained on non-reproduceable experimental datasets, their predictions may not generalize.

Limited sharing of experimental data in publications also acts as a bottleneck for the reproducibility and validation of results within the research community. Therefore, researchers practice data (*i.e.*, datasets, methodologies, and metadata) sharing on platforms such as Zenodo, Figshare, Kaggle, or GitHub to promote reproducing experiments. When sharing information on data-driven methods such as ML, not only is it important to provide model weights, but also information such as training and testing datasets, the source of the datasets, dataset metadata, data cleaning procedures, data preprocessing steps, and training procedures (*e.g.*, feature selection and hyperparameter optimization).

2.2 Notable computational studies

2.2.1 Water, CO_2, and nitrogen electrolysis. Water electrolysis is a potentially greener alternative to steam reforming and coal gasification for making hydrogen fuel.[11,93] In the HER, protons from split water are reduced to produce H_2 gas.[94] The electrochemical reduction of CO_2, eCO_2RR, can produce a variety of carbon products such as hydrocarbons and alcohols, therefore being a possible closed-loop, chemical production process.[95] Nitrogen electrolysis or the nitrogen reduction reaction (NRR) refers to breaking the N_2 triple bond to make ammonia as an alternative to the Haber–Bosch method.[96] A big challenge with water electrolysis and eCO_2RR is finding materials that are less expensive and more stable so that their respective products can become more cost-competitive. As for the NRR, breaking the triple bond requires a highly active catalyst and a lot of energy. However, most reported materials have yet to produce significant current densities to make this alternative attractive.[97] Hence, applying HT methods for these fields greatly benefits their advancement.

At first, Mao *et al.* used the aforementioned H adsorption energy (ΔG_H) as the descriptor for the HER activity of Cu-based alloy nanoclusters with varying dopant concentrations.[56] The DFT study depicted that changing the dopant concentration evolved the structure of the alloy, which affected the excess energy (structure stability), the number of active sites, and the ΔG_H. From here, the authors figured that doping created a significant charge difference between the Cu vertex and edge sites and associated that with ΔG_H. Therefore, the researchers proposed the average partial atomic charge difference between these two adjacent sites, ΔQ_{Cu-Cu}, as a new descriptor that is easier to compute than ΔG_H. Finding a more accessible descriptor to compute reduces the costs of computational material discovery *via* DFT, thus making this method more accessible to all researchers.

Yohannes *et al.* evaluated transition metal nitrides as eCO_2RR catalysts using activity, selectivity, and stability DFT descriptors.[37] Again, adsorption energies, ΔG_{CO} and ΔG_{CHO}, are used as descriptors to mark activity toward C_1 products. Additionally, the authors uncommonly applied the adsorption energy of hydroxyl, ΔG_{OH}, to predict the stability of the catalyst against –OH poisoning. If bound too strongly, the *OH can stay on the surface and hinder active sites for eCO_2RR or reduce to water, thus stealing electrons and decreasing efficiency. Moreover, the HER is parasitic to eCO_2RR, so the authors again used H adsorption energy, ΔG_H, to predict eCO_2RR selectivity on a catalyst surface over the HER. High selectivity (Faradaic efficiency) for eCO_2RR reduces downstream separation costs, making the HER an undesired side reaction. With these descriptors, several Co-, Cr-, and Ti-based nitrides were suggested as catalysts worth further eCO_2RR experimentation. This study showcases how adsorption energy can be applied in unique ways to probe properties outside of activity.

While most researchers funnel down materials with each step having a new criterion (single-objective approach), Kavalsky *et al.* performed a multiobjective optimization combining DFT and ML methods to discover single-atom alloy (SAA) electrocatalysts for the NRR.[57] The researchers first employed sequential learning to train an ML model and build their full catalyst design space, which was then evaluated using DFT as implemented in the Autocat workflow shown in Fig. 2.[98] The

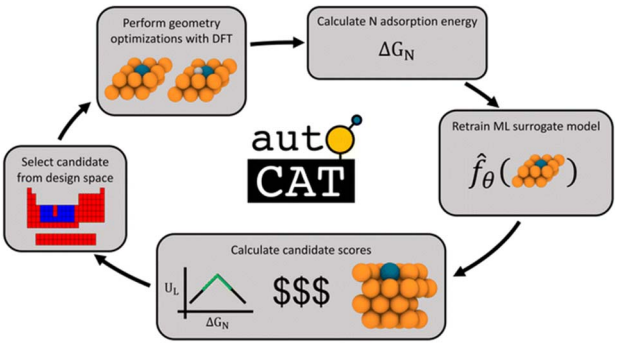

Fig. 2 Closed-loop workflow for discovery of SAA electrocatalysts. The workflow starts from selection of a material from the design space, followed by structure geometry optimization and the subsequent N-atom adsorption calculation. The calculated results are used to retrain the ML surrogate model, which encodes activity, cost, and stability metrics and outputs the candidate scores. The highest scoring candidate is selected for evaluation. Reproduced with permission from ref. 98. Copyright 2024 Royal Society of Chemistry.

scores of three crucial performance metrics, stability, cost, and activity, were evaluated simultaneously to help discover electrocatalysts for nitrogen reduction. The chosen multiobjective descriptors were segregation energy (stability), the Herfindahl–Hirschman index (material cost), and ΔG_N (activity), which presented Zr_1Cr, Au_1Re, Ag_1Re, Ti_1Fe, and Hf_1Cr as promising performers (note that X_1Y denotes a single dopant of species X into a host of species Y in the context of an SAA as shown in Table 1). The authors stated that this tactic catches suitable materials that single-objective screening would typically omit. This work indicated that considering small compromises in specific material properties when constructing such models can strengthen discovery.

2.2.2 Fuel cells and batteries. The use of fuel cells has been proposed as an alternative to electricity production from fossil fuel-based methods, especially for commercial vehicles and transit. Although there are many different types, the hydrogen fuel cell is the most popular since its only emission is water and its fuel, hydrogen, is the single most abundant molecule on earth. In a hydrogen fuel cell, the hydrogen oxidation reaction (HOR) occurs at the anode, where hydrogen is oxidized to protons, which are then transported to the cathode side. At the cathode, the oxygen reduction reaction (ORR) takes place, where oxygen reacts with the protons and is reduced to water. The most common complementary reactions in a fuel cell are the oxygen evolution reaction (OER) and HER. The OER is also used as the oxidation half-reaction for water and CO_2 electrolysis. All these reactions—the HOR, HER, ORR, and OER—typically require precious metal catalysts such as Pt, Ru, Pd, and Ir. This necessity makes these reactions attractive for study using HT methods to discover cheaper, high-performing electrocatalyst materials.

Unlike most materials science labs focused on HT screening catalysts, Tran *et al.* used ML to explore polymers for ionomers and membranes in fuel cells.[69] This study aimed to find alternatives to Nafion, the state-of-the-art polymeric material for fuel cells and electrolyzers. Although proven effective in many circumstances, Nafion, a cation exchange ionomer, is expensive and not always best suited for its application. Replacing Nafion could also address safety concerns. Nafion is classified as a per- and polyfluoroalkyl substance, PFAS, which presents health effects due to its slow break down and persistence in the environment; traces of PFASs have been found in the blood of people and animals globally.[99,100] In any case, the authors used eight key properties (*e.g.*, ion conductivity, gas permeability, band gap, *etc.*) of Nafion as a benchmark for screening 30 000 previously reported polymers using multiple ML models. The authors identified 60 new polymers as possible replacements because their predicted properties outperformed those of Nafion. Yet, this study did not include any safety-centered metrics to evaluate candidates for health effects and handling, identifying a need to improve this method. This work's strategy is enabled by polymer informatics, hoping to further leverage ML for future studies in discovering unencountered polymers.

Large-scale batteries, both solid-state and redox flow, can function as electrical grid stabilizers during periods of low demand by storing excess energy supply for later use. This application requires battery materials to be resilient against multiple charges and discharges during their lifetime. Therefore, researchers have employed HT methods to scope out new battery electrolytes with multiple oxidation states for charge storage, high ionic conductivity, wide potential ranges for stability, and high earth abundance for costs.

Researchers often use the so-called HOMO–LUMO gap, which is an electronic property calculated as the difference between the highest occupied molecular orbital (HOMO) and the lowest unoccupied molecular orbital (LUMO), to assess the stability descriptor of battery electrolytes' solvents. Generally, a larger HOMO–LUMO gap is associated with more stable materials. This approach enables rapid assessment without requiring the optimization of oxidized or reduced electrolyte molecules. However, the Knap lab indicated the impact of molecular geometry relaxation during electrolyte oxidation, providing evidence by screening the electrochemical stability of 100 carbonate and 300 phosphate molecules as solvents for Li battery electrolytes.[70] Initially, the Knap lab's HT screening model focused on the oxidation and reduction potentials of isolated solvent molecules to determine their stability windows. Additionally, the model involved geometry optimization as some less stable (smaller gap) molecular formations of the electrolyte decomposed under different conditions. After presenting these results, the authors commented on their initial method and stated the importance of also including intermolecular interactions with other solvent molecules as well as Li ions. To enhance the prediction of the electrochemical stability of isolated electrolyte, the authors explicitly incorporated solvent molecules into their models. This approach allowed the authors to simulate H-abstraction and Li^+ semi-fluorination scenarios more accurately. While preferred DFT models typically center on simple representations and minimal intermolecular interactions, making them a straightforward yet insightful tool, Knap *et al.* noted that more accurate results

Table 2 Summary of experimental HT methods for electrochemical material discovery, production, synthesis, characterization, and analysis. All acronyms not previously mentioned in the text are defined in table footnotes

Material	Rxn(s)	HT application	Cell(s)	Deposition method	Best material(s)	Year	Ref.
Catalyst	eCO_2RR	Electroanalysis	3-Electrode	Automated liquid handler deposition robot	$Au_6Ag_2Cu_2$	2021	101
Catalyst	eCO_2RR	Electroanalysis	SECM[a]	Polishing	Sn/SnO_2	2020	102
Catalyst	eCO_2RR	Synthesis	H-cell	Spin cast	$Cu_{0.8}In_{0.2}$	2017	103
Catalyst	eCO_2RR	Material ID Electroanalysis	SFC	Magnetron sputtering	Pd–Zn	2019	104
Catalyst	HER	Production	3-Electrode	Dip coating	HC–MoS_2/Mo_2C	2020	105
Catalyst	HER	Electroanalysis	3-Electrode	Sputtering	$Pd_{63}Ni_{16}Fe_{21}$	2023	106
Catalyst	HER	Electroanalysis	3-Electrode	Sputtering	$Ni_{56.5}Co_{35}Ti_{8.5}$	2022	107
Catalyst	HER	Synthesis Characterization Electroanalysis	SDC	Sputtering	$Co_{56}Cr_8Fe_{19}Mo_7Ni_{10}$	2022	108
Catalyst	HER	Material ID	SDC Flow cell	Co-sputtering Spray-coating	$Co_{23}Cu_{34}Mo_{17}Pd_{14}Re_{12}$	2024	109
Catalyst	HER OER	Synthesis	PEM[b] and MEA[c]	Spark ablation	IrO_2	2022	110
Catalyst	OER	Synthesis Electroanalysis	Flow cell 3-Electrode	Drop casted	CoO Co(50%)Ni(50%) CoNiFe (up to 12.5%)	2022	111
Catalyst	OER	Electroanalysis	SDC	Drop casted	Not stated	2013	112
Catalyst	OER	Material ID Electroanalysis Characterization	SDC	Ink jet printing-assisted co-op assembly	$Fe_{O.3}Ni_{0.7}O_x$ $Fe_{0.23}C_{0.13}Ni_{0.07}Ti_{0.57}O_x$	2013	113
Catalyst	OER	Material ID Electroanalysis	SDC RDE[d]	Inkjet printing	$Ni_{30}Fe_7Co_{20}Ce_{43}O_x$	2014	114
Catalyst	OER	Material ID Electroanalysis	SDC RDE	Inkjet printing	$(Ni_{0.1}La_{0.1}Co_{0.3}Ce_{0.5})O_x$	2014	115
Catalyst	OER	Material ID Electroanalysis	SDC	Reactive co-sputtering	$Mn_{0.4}Sb_{0.22}Sn_{0.08}Ti_{0.3}$	2023	116
Catalyst	OER	Synthesis Electroanalysis	25 compartment 3 electrode cell	Automated pipetting robot	$La_{0.2}Sr_{0.8}Fe_{1-y}Co_yO_3$	2023	117
Catalyst	OER	Characterization Electroanalysis	SDC	Combinatorial reactive magnetron co-sputtering	$Ni_{1-y-z}Fe_yCr_zO_x$	2017	118
Catalyst	OER ORR	Synthesis	Joule heating method (synthesis) 3-Electrode cell	Not stated	Fe–CoO	2023	119
Catalyst	ORR	Electroanalysis	SFC	N/A	Not stated	2012	120
Catalyst	ORR	Synthesis Electroanalysis	SDC RDE RRDE	Drop cast printing	PtPdRhNi PtPdFeCoNi	2020	121
Catalyst	ORR	Electroanalysis	Scanning gas diffusion electrode half cell	Ultrasonic spray coating	Pt/C	2024	122
Catalyst	ORR HER	Material ID Electroanalysis	SDC	Co-sputtering	$Ti_{14}Ni_{17}Cu_{16}Zr_{21}Pd_{17}Hf_{15}$ (ORR) $Ti_{11}Ni_{13}Cu_{18}Zr_{17}Pd_{19}Hf_{22}$ (HER)	2022	123
Catalyst	HER OER IPA oxidation	Synthesis	Customized PEM electrolyzer	Spark ablation	NiFe Ni(O)OH	2020	124
Catalyst	IPA oxidation	Electroanalysis	SDC	Combinatorial magnetron co-sputtering Drop cast	$Pt_1Ru_1Ir_{1.5}/C$	2023	125
Catalyst	MOR	Electroanalysis	Customized 25 compartment MEA	Not stated	PtRu	2002	126
Gas diffusion electrode	eCO_2RR	Electroanalysis	AutoGDE (SFC)	Evaporation	N/A	2024	127
Multiple	eCO_2RR HER	Electroanalysis	SFC	N/A	Cu foil	2014	128

[a] Scanning electrochemical microscopy cell. [b] Proton exchange membrane. [c] Membrane electrode assembly cell. [d] Rotating disk electrode cell.

require more extensive and computationally intensive DFT calculations that may be beyond the reach of most researchers.

3. Experimental methods

The methodology for most experimental electrochemical tests involves material synthesis or preparation, material deposition or casting, electroanalysis, and pre- and post-testing characterization. The step-by-step process very much depends on the reaction and the type of material being tested. Therefore, unlike computational studies, setups across labs can vary vastly, leading to many customized setups for both benchtop and HT experimentation. While insightful, this variety in experimental setups hinders data comparison across research labs. Yet, researchers thoroughly detailing their methods and custom setups in publications stimulate more similarities as others incorporate proven procedures into their own setups. Meanwhile, continuous efforts to commercialize HT experimental setups will drive method standardization, thus minimizing differences in procedures from lab to lab. Table 2 summarizes the experimental literature we evaluated in this review, including the material type, the cell used, and the top-performing material(s). Table S2† provides more details about the methods including substrates and electrolytes. This section highlights notable experimental setups and methods for electrochemical applications.

3.1 Scanning cells

The use of scanning cells (flow, droplet, and electrochemical microscopy) may be the most effective approach for HT electroanalysis of electrochemical materials. Various labs have established this technique where a motorized, programmable stage hosting samples of materials is moved to electrically come into contact with a stationary cell.[102,109,112–116,118,120,121,123,125] A few examples of scanning cells for HT screening are depicted in Fig. 3. Although typically catalysts, other sample materials for testing may be different membranes, substrates, or ionomers. At each sample, the cell can conduct a myriad of electrochemical tests before moving on. The number of samples depends on the size and reach of the stage (size of the setup) and the individual sample size, meaning that tens or hundreds of compositions can be screened in the time it traditionally takes to test two or three. Researchers who have built custom scanning cells initially performed repeatability experiments (at least 3) to ensure good reproducibility, validate their setups, and minimize error before collecting data.[112,127,128] Small deviations may arise from problems such as bubble formation and material degradation, but overall, these researchers claim high reproducibility when testing with scanning cells, possibly due to lowered human error. Gregoire *et al.* concluded that the smaller droplet size, and thus a smaller working electrode area, leads to this improved reproducibility.[112]

The Joint Center for Artificial Photosynthesis, JCAP, designed and built its own scanning droplet cell (SDC) to conduct HT screening and mapping mainly of OER catalysts.[112–116] This setup, displayed in Fig. 3a, invokes a stationary 3-electrode cell, equipped with counter and reference electrodes, that comes in electrical contact with the working electrode *via* a controlled-area electrolyte droplet. Again, the working electrode sits on a motorized *X*–*Y* stage, which moves to change the sample. The cell does not press down on the working electrode substrate and thus is an open system exposed to the atmosphere, which is not a concern for studying the OER. The researchers created compositional libraries of catalysts using inkjet printing or co-sputtering and then mapped them with the SDC. The publications from this group boast automated screening of anywhere from 100 to 5400 different catalyst compositions and the creation of their corresponding activity maps (current *vs.* composition). Their work has led to the proposal of several different candidate materials for OER catalysis that are worth exploring further.

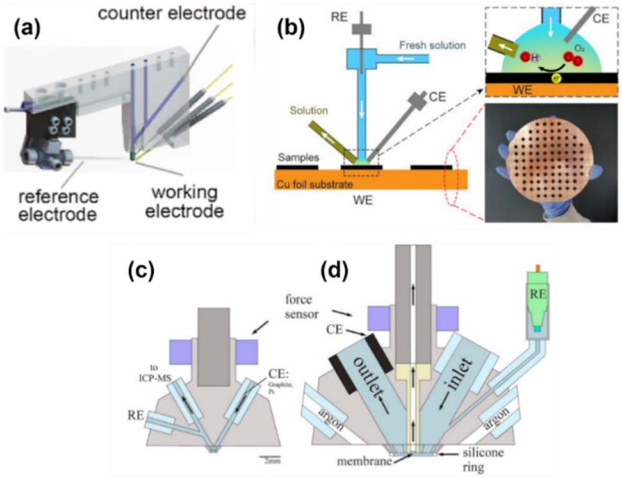

Fig. 3 Examples of scanning cells for HT material screening. (a) Scanning droplet developed at the JCAP. Reproduced with permission from ref. 112. Copyright 2023 Royal Society of Chemistry. (b) Scanning droplet cell with expanded views of (top) droplet contacting the sample and (bottom) compositional library deposited on a Cu foil substrate. Reproduced with permission from ref. 121. Copyright 2020 National Academy of Sciences. Scanning flow cells with (c) an incorporated channel for inline ICP-MS and (d) an outlet for online EC-MS measurements and surrounding argon to block air diffusion. Reproduced with permission from ref. 122. Copyright 2014 AIP Publishing LLC.

Unlike a SDC, a scanning flow cell (SFC), equipped with a gasket, touches down onto the working electrode surface to create a seal and thus a closed system.[104,120,122,127,128] The electrolyte is ushered to and from the surface while tests are conducted instead of staying stationary in a droplet. SFCs are better for reactions where purity or oxygen reactivity may be a concern or reactions that require product quantification, like eCO_2RR. Mayrhofer *et al.* reported a customized SFC for testing ORR catalysts.[120] Their initial reported design had argon surrounding the cell tip to discourage air diffusion, and they conducted proof-of-concept experiments to determine catalyst geometric area, O_2 saturation time, and any flaws in the design. This SFC was improved upon by adding online product analysis *via* electrochemical mass spectroscopy (EC-MS)[128] and later gas flow and dissolution analysis *via* inductively coupled plasma-mass

spectrometer (ICP-MS), as shown in Fig. 3c and d.[122] Screening with SFCs typically takes longer than that with SDCs because of the extra time needed to properly make contact and to clean the surface after detaching. Even so, SFCs are an imperative tool for materials screening and discovery as many reactions, including those discussed here (*e.g.*, the HER eCO_2RR), require closed systems for proper electroanalysis.

Although not consistent with the scope of this review, we would like to highlight that many labs have developed successful electrochemical scanning cells for other studies, such as corrosion or photoelectrochemistry, which are also pertinent to material development and mitigation efforts.[129–137]

3.2 Multi-compartmental and optical setups

Up to this point, we have discussed HT experimental methods conducted sequentially. One after another, a cell comes into contact with a sample and then evaluates the material's performance. Nevertheless, some laboratories have transitioned from single cell setups to advanced HT systems to assess samples in parallel, commonly referred to as multi-compartmental setups.

One example of these setups is the one developed and patented by Smotkin *et al.*, which consists of a segmented MEA-type fuel cell capable of screening 25 catalyst samples at once.[126,138–140] While the samples shared a common counter electrode and the reactant flowed to each in series, each catalyst in the array was isolated using a Teflon gasket and equipped with its own sensor to control potential and measure current. Instead of a multi-channel potentiostat, this study utilizes a voltage follower, a current follower, a programmable computer card, and LabView to set the potential output and acquire the current. The authors commented on their initial design and pointed out areas of improvement, such as the need to make sample preparation scalable. Although their reports focus mainly on bimetallic PtRu catalysts, their setup can easily be adapted to screen a library of different materials simultaneously.

Certain setups rely on optical techniques to screen samples for electrolysis. These optical methods incorporate cameras to visualize all samples simultaneously and interpret their reaction kinetics. For instance, Zou *et al.* designed a HT bubble screening tool to study Pd–Ni–Fe alloys for the HER.[106] Co-sputtering all metals at once created a compositional library on a Cu electrode, which was later submerged in a glass 3-electrode cell for testing. The researchers positioned a camera at the bottom of the cell to record the gaseous H_2 bubbles forming from the HER across the electrode. Then, the authors associated the bubble diameter (volume) with the activity at that position and composition, as shown in Fig. 4a. Hence, the larger the bubble, the better the activity, resulting in an activity map. The authors discovered $Pd_{63}Ni_{16}Fe_{21}$ to be the optimal composition for their proposed alloy. Moreover, Hitt *et al.* observed eCO_2RR activity of an array of 72 different catalyst compositions using a camera positioned over a customized gas-fed 3-electrode cell with an optically transparent window (Fig. 4b).[101] Here, the authors added a pH indicator to the electrolyte and left it unstirred. Thus, as eCO_2RR proceeded, over all catalyst samples at various applied potentials and protons were consumed, the pH increased, and the color of the electrolyte

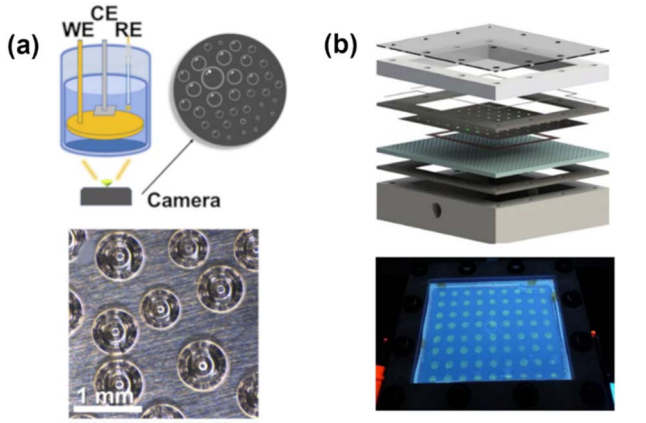

Fig. 4 (a) HT bubble screening setup for measuring HER activity with an example of the camera view below. The camera below the working electrode allows for visualization of the H_2 bubbles forming on the catalyst compositional library. WE: working electrode; CE: counter electrode; RE: reference electrode. Reproduced with permission from ref. 106. Copyright 2023 Elsevier B.V. (b) An exploded (top) and live (bottom) view of a custom, 72-sample HT cell for measuring eCO_2RR activity based on color change with a pH indicator. The authors validated the setup by depositing the same catalyst in each location and ensuring that the pH color did not vary. Reproduced with permission from ref. 101. Copyright 2021 Springer Nature Ltd.

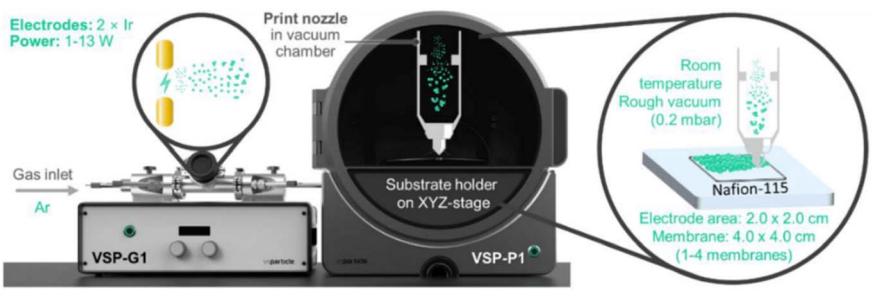

Fig. 5 Schematic of the VSParticle nanoparticle printing technology. A certain wattage is applied to metal electrodes which causes the metal to ablate and particles to detach. The particles agglomerate to form nanoparticles as they are carried by inert Ar to a vacuum chamber where they are printed *via* a nozzle onto a substrate of choice held by an *XYZ*-stage. Reproduced with permission from ref. 110. Copyright 2022 MDPI.

changed. The onset of the color change was related to the onset potential of eCO_2RR for that catalyst. Lower values suggested a more active catalyst, and the authors created an activity map with their data. $Au_6Ag_2Cu_2$ was the most active catalyst for CO production from eCO_2RR. Although both examples, the bubble screening and pH sensing, demonstrate rapid catalyst screening, they cannot perform product quantification and assume uniform potential distribution across the electrode. Yet, these studies aimed to quickly identify the best material, which they succeeded in and followed up with a full electroanalysis of that material in a traditional single cell.

3.3 Other notable efforts

Many material deposition methods listed in Table 2 involve a liquid phase by which the material is first formulated into an ink, solution, or dispersion (*e.g.*, drop-casting and spray coating). Sputtering, a type of physical vapor deposition, is another common method for depositing metal particles, specifically, but does not require first dispersing the metal in a solvent. The advantages of sputtering include greater control of particle size, composition, thickness, and loading than wet deposition methods, and it is possible to create compositional libraries with this technique.[141] As an alternative to sputtering and other deposition methods, a Dutch company, VSParticle, designed a nano-printer for printing (semi)conductive particles. This innovative technology, depicted in Fig. 5, employs spark ablation followed by impaction to form and deposit nanoparticles.[110,124] While sputtering typically requires the target material and a high-energy ion source by way of ionizing Ar to Ar^+, spark ablation only requires the target metal, electricity, and an inert gas and thus is a "chemical-free" deposition. With adjustable parameters such as voltage, current, flow rate, and nozzle size, this nano-printer boasts the ability to make highly tunable nanoparticle films of varying compositions, thicknesses, loadings, and particle sizes in a matter of hours. In fact, Becker *et al.* printed 64 (8×8) NiFe electrodes of various compositions to test in their customized cell, with each electrode only taking 1–320 seconds to print.[124] In a different study, Sapountzi *et al.* fabricated IrO_2-coated membranes using spark ablation for conducting the OER at a fifth of the loading (cost) compared to commercially available catalyst coated membranes (CCMs),[110] underscoring the importance of the deposition method when designing cost-competitive materials.

The materials listed in Table 2 have potential for use in a myriad of electrochemical applications, yet most were studied at the lab scale. If a certain catalyst or electrolyte, for example, proves performative and cost-effective, then the next step would be scaling up its production. Zhang *et al.* took that next step by reporting HT production of two-dimensional MoS_2 flakes for fabricating thermally treated MoS_2/Mo_2C (HC–MoS_2/Mo_2C) catalyst for the HER.[105] The reported method involved extracting raw Mo concentrates (MoS_2, MoO_2, MoO_3, and others) from an active open pit mine and exfoliating it with Mo_2C to form two-dimensional MoS_2 flakes. These MoS_2 flakes were then dispersed in water to make an ink for dip-coating a high-surface area Cu foam substrate in. Lastly, the dipped substrate was heated in a CH_4/H_2 mixture to form the final electrode which exhibited a high activity of 1 A cm^{-2} at an overpotential of 347 mV. While HC–MoS_2/Mo_2C's performance is comparable to that of state-of-the-art Pt/C, the authors determined that the price of the Mo concentrate precursor is $5\times$ cheaper than that of Pt. This reduction in material cost plus their HT method made HC–MoS_2/Mo_2C $\sim 30\times$ cheaper than commercial Pt/C. Choosing to omit any purification steps helped reduce the cost of production while showing the resilience of the catalyst even with the existence of impurities originating from the mine. The authors anticipate their method being extended to other natural materials for HT electrocatalyst production.

3.4 Analytical characterization

Physical characterization performed before and after electroanalysis plays an imperative role in scientific methods of HT material discovery. Researchers incorporate analytical characterization (morphology, composition, crystallization, *etc.*) in traditional benchtop studies to answer questions about a material's performance. Thus, HT experimental methods also require HT characterization techniques to identify the most feasible materials for electrochemical applications. Scientists have innovated new techniques to address speed-related bottlenecks in common analytical methods such as X-ray diffraction (XRD) and X-ray fluorescence.[142,143] Incorporating multi-sample and automated stages into instruments increases the number of samples that can be characterized while reducing analysis time. Parallel chambers in systems for Fourier-transform infrared spectroscopy, ultraviolet-visible spectroscopy, and N_2 adsorption/desorption allow for samples to be loaded and analyzed simultaneously. Various labs [and manufacturers] have also employed robotic arms for machine tending to automate menial measurements such as mass loading to increase process efficiency.[144] Machine manufacturers for these common techniques have already rolled out their HT versions of their instruments.[145–148] Taking it a step further, researchers have gone so far as to start incorporating ML into physical characterization techniques to improve their efficacy. Szymanski *et al.* developed an autonomous and adaptive XRD by coupling ML with a physical diffractor to hasten phase detection, leading to *in situ* identification of short-lived intermediates during solid-state reactions.[149] This application serves as a nice segue into the following section where we discuss combined computational and experimental methods.

4. Combined methods

Synergistic approaches that integrate both computational and experimental methods are essential for accelerating material discovery. While conducting studies that employ both techniques requires greater effort, the resulting insights are often significantly deeper and more insightful. There are several approaches to combining these techniques, rather than a single recipe. For instance, experiments can be performed first to generate datasets that train ML models through supervised learning. Additionally, a ML or DFT model can suggest

Table 3 Summary of HT studies that combine both computational and experimental methods for material discovery. All acronyms not previously mentioned in the text are defined in table footnotes

Material	Rxn(s)	Cell(s)	Model(s) DFT	Model(s) ML	DFT descriptor(s)	ML algorithm	Top material(s)	Year	Ref.
Catalyst	eCO_2RR	3-Electrode	✓		Pore limited diameter Coordination of unsaturated metal sites Adsorption capacity	N/A	MOFs[a] GAFRUD CAJQEL cg400449c	2022	150
Catalyst	eCO_2RR	Flow cell	✓	✓	ΔG_{CO} ΔG_H Formation energy	GNN	CuAl	2024	79
Catalyst	HER	N/A	✓		ΔG_H	N/A	BiPt alloy	2006	151
Catalyst	HER	RDE	✓		A-site ionic electronegativity	N/A	$(Gd_{0.5}La_{0.5})BaCo_2O_{5.5+\delta}$	2019	152
Catalyst	OER	H-cell		✓	N/A	BO	$Co_{0.2}Mn_{0.7}Ni_{0.1}O_x$ $Co_{0.6}Fe_{0.3}Ni_{0.1}O_x$	2023	153
Catalyst	OER	3-Electrode	✓	✓	Bond length between metal ions & atom 2 Average charge of the active site Electron affinity for the metal center Ionic radius of the active site atom	GBR	Ni covalent organic framework	2021	154
Catalyst	OER	3-Electrode	✓		Decomposition energy Pourbaix (Nernst equation) Cubic *Pm3m* space group	N/A	$LaAlO_3$	2022	78
Catalyst	OER	3-Electrode	✓	✓	Electronic structure (O 2p band center, M 3d band center, and Bader charges) ΔG_O ΔG_{OH} ΔG_{OOH}	RF BO LAS	$Co_{2.5}Ga_{0.5}O_4$	2024	155
Catalyst	ORR	Multi-channel (4) flow double electrode cell RDE		✓	N/A	SVM GBR	$Fe_{4.8\%}Zn_{95.2\%}$	2020	156
Catalyst	ORR	RRDE[b]	✓		ΔG_{OOH}	N/A	Cobalt porphyrin	2022	157
Catalyst	ORR	SECM RRDE	✓		ΔG_O on Fe	N/A	FeNiCuCoPt/CNFs	2024	158
Catalyst	ORR	MEA	✓		d-Band center ΔG_O ΔG_{OH}	N/A	Pt_3Co	2020	159
Catalyst	ORR OER	Sealed glass cell	✓		Dissolution reaction energy Energy above the convex hull	N/A	26 OER oxide candidates 2 ORR oxide candidates	2022	80
Electrolyte	HER ORR OER	Button cell	✓		Oxygen vacancy ΔG_{CO_2} Hydration energy ΔG_{H_2O}	N/A	$BaSn_xCe_{0.8-x}Yb_{0.2}O_{3-\delta}$	2024	160
Electrolyte			✓	✓	Li mole fraction — Li diffusivity Band gap — Cost Redox potential — Shear modulus Stability — Density	GNN	$Na_xLi_{3-x}YCl_6$	2024	161

Table 3 (*Contd.*)

Material	Rxn(s)	Cell(s)	Model(s) DFT	Model(s) ML	DFT descriptor(s)	ML algorithm	Top material(s)	Year	Ref.
Electrolyte				✓	N/A	LR[c]	1,4-Dioxane	2022	162
						GPR			
Electrolyte			✓	✓	N/A	BO	dioxane : dimethyl sulfoxide @ 0.8 : 0.2 vol%	2024	163
Electrolyte			✓		Energy above the convex hull Reaction energy Band gap Ionic conductivity	N/A	Li_3OCl	2025	164
Electrolyte			✓		Li-phonon band center	N/A	Li_3ErCl_6 and 17 other candidates	2019	165

[a] Metal organic framework. [b] Rotating ring disk electrode. [c] LR: linear regression.

materials for subsequent synthesis and testing to validate their effectiveness. This new data can then be reintroduced into the ML model, enhancing its capabilities. Hence, by combining computational and experimental methods, researchers can also develop iterative processes to design and discover materials. This section discusses remarkable work reported in the literature in which computational methods are incorporated into experimental setups. Table 3 summarizes all the literature with combined computational and experimental methods we evaluated in this review with information such as the model, descriptor, material type, cell, and the top performing material(s). A more detailed version of this table is provided in the ESI.†

4.1 Computational screening followed by synthesis

Recently, Microsoft, in collaboration with a research group from the Pacific Northwest National Laboratory (PNNL), reported the discovery of electrolytes for solid state batteries driven by high-performance, cloud-based computing.[161] Starting with known crystal structures, the authors chose 54 elements and obtained their common oxidation states to perform ionic substitution in the pre-existing materials. All in all, over 32.5 million initial structural candidates were generated for screening. From here, the study moves to a 10-step funneling method to evaluate the selected candidates. The first step narrowed down materials using their phase stability E_{hull} < 50 meV per atom (E_{hull} is the relative energy above the convex hull and obtained by using ML-based potentials[166]), bringing the number down to under 6 × 10^5 (Fig. 6a and b). The following levels encompassed criteria pertaining to solid electrolytes such as Li conductivity, redox potential, and cost. Distinctively though, each criterion step is performed with either ML or DFT based on the need for quicker (cheaper) screening or higher accuracy, respectively. Essentially, this strategy demonstrates using ML for a large dataset because it requires less computing time and then switching to DFT once the dataset has been tapered down for more reliable but not excessively expensive analysis. Consequently, the authors identified 18 electrolytes that had not been previously reported and focused on four to further investigate through synthesis and characterization. The top candidate was $Na_xLi_{3-x}YCl_6$ based on its structures and conductivities, making it a suitable choice for a solid electrolyte (Fig. 6c and d). Even with such an expansive search and a detailed screening, the authors concluded that relaxing the criteria for the filters could help detect additional candidates, which echoes Kavalsky *et al.*'s call to consider small compromises when screening materials.[57]

Sarwar *et al.* recently performed HT-DFT calculations to study the electrocatalytic activity and stability of over 2000 Pt_3M bimetallic alloys for the ORR, where M represents a list of 21 metals.[159] The researchers evaluated the effectiveness of descriptors such as the surface d-band center and ΔG_O and investigated the impact of M surface segregation under vacuum and O- and OH-induced conditions. By conducting experimental studies, the authors were then able to correlate the O-induced segregation energy with the percentage of M metal loss (leaching). Moreover, the computational findings indicated

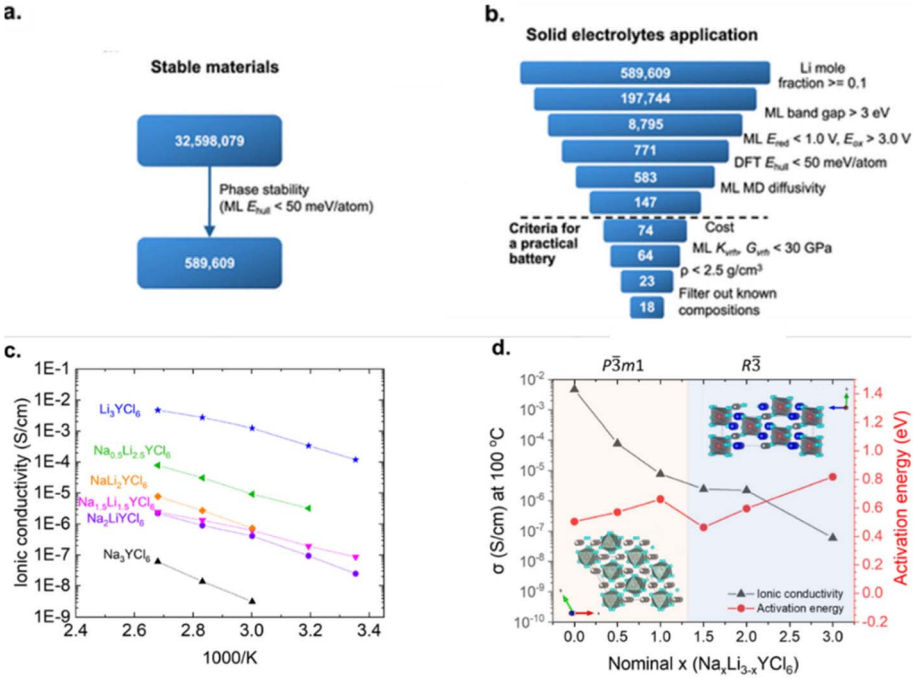

Fig. 6 (a) Material screening based on phase stability. (b) Workflow of discovering solid electrolytes with miscellaneous screening criteria. (c) Ionic conductivities of $Na_xLi_{3-x}YCl_6$ measured at different temperatures. (d) Relationship between the crystal structure and ionic conductivity. Reproduced with permission from ref. 161. Copyright 2024 American Chemical Society.

that the d-band center might not be a reliable descriptor once surface segregation effects occur as the d-band center could not predict the decrease in ORR activity once the M metal migrated to the surface (leaching). This phenomenon was confirmed with the electroanalysis data as ORR activity displayed an enhanced correlation with ΔG_O compared with the d-band center. Therefore, the authors concluded that ΔG_O could serve as a better descriptor when considering the surface and binding energy changes post-segregation. This discovery suggests that some descriptors may be suited for certain catalyst morphologies, which could motivate more tailored DFT calculations for specific material configurations.

Coupling experimentation and computation for Karim *et al.* involved conducting experiments not only after but also before creating their ML model.[156] At first, the researchers prepared 36 different catalyst samples using a HT automated synthesis platform and followed up by testing them all for ORR activity. The electrochemical cell for running the ORR was a customized multi-channel flow cell capable of screening four catalyst samples at a time. Out of the resulting dataset, 60–80% were used to train five ML models with the synthesis parameters (Fe atomic%, pyrolysis T, and Fe precursor) as inputs. Each ML model utilized a different algorithm to help find the minimal (optimal) RMSE and mean absolute percentage error. The best-performing algorithms were gradient boosting and support vector regressions. From here, the authors used these two optimal models to predict ORR activity as a function of the synthesis parameters, which represents outputting new catalysts. Taking it a step further, the researchers synthesized new catalysts using these predicted parameters and tested them for ORR activity to validate the model. The new material not only met but exceeded its modeled performance. Continuing this method of synthesis, testing, training, and predicting could allow the authors to iteratively improve their model and find the next best materials for the ORR before expanding it to other reactions.

4.2 Integrated robotic platforms

Robotic platforms have been introduced in various applications to increase experimental throughput, minimize human error, and improve researchers' safety regarding hazardous materials. Moreover, robotic platforms' speed provides larger initial datasets for training ML models and allows suggested materials to be synthesized, tested, and fed back into the model simultaneously in batches rather than one by one with traditional benchtop chemistry.

To find the optimal solvent for electrolytes in redox flow batteries, researchers at PNNL and Argonne National Laboratory developed an automated workflow that linked robotic HT synthesis and analysis with ML, as shown in Fig. 7.[163] In short, they built a closed-loop, ML-guided HT experimentation setup to further speed up screening. To start their study, the authors listed 22 possible solvent candidates and then created an additional 2079 candidates based on binary mixtures of various volume ratios of the original 22. Next, their automated robotic platform synthesized 58 of these candidates (both singular and binary solvents) for model training at a rate of ~39 min per sample. Each electrolyte sample was prepped for nuclear magnetic resonance (NMR) and then manually transported to

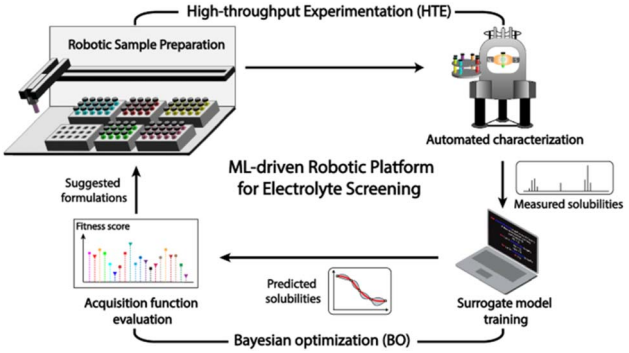

Fig. 7 Schematic of the closed-loop electrolyte screening process based on an ML-guided HT experimentation platform. Reproduced with permission from ref. 163. Copyright 2024 Springer Nature Ltd.

an auto-sampling NMR machine for quantitative analysis of ^{1}H NMR spectra. The integrated peak areas were used to calculate solubility. The results from these 58 samples first trained a surrogate model to determine whether Bayesian Optimization (BO), a type of AL, would be effective with this dataset. The surrogate model training was then validated with 40 additional solvent candidates and then it was asked to identify the solvent with the highest solubility out of its 98 samples. Once the surrogate model was verified, the authors deployed BO to complete their ML-guided, closed-loop setup and then ran three cycles. Each cycle started with (1) the model suggesting 40 solvent samples, (2) synthesis and evaluation as described above, and (3) feeding the results back into the model. BO only took one cycle to identify dioxane : dimethyl sulfoxide @ 0.8 : 0.2 vol% as the solvent with the highest solubility. Since the subsequent cycles did not detect a better solvent, the authors halted their evaluation meaning that their model only needed 218 measurements from the >2000 sample dataset to output the optimal solvents and solvent ratio. The detailed automated HTE system for solubility measurement is given in Fig. 8. This demonstration of BO underscores how active (machine) learning can drive experimentation toward minimizing the time and calculations (cost) needed to screen larger datasets and discover materials.

Understanding that the search space for catalyst multi-element electrocatalysts is too vast even for automated HT robotic platforms, Kodera and Sayama also incorporated ML into their robot system to explore catalysts for the OER and HClO production using seawater.[153] Their fully automatic robot was able to conduct synthesis and electroanalysis of 88 catalyst samples per day. The authors started by setting their system to synthesize and analyze different combinations of four elements (Co, Mn, Fe, and Ni), chosen based on their reported performance, to obtain 286 data entries. With these data, the authors investigated composition optimization using BO by having the ML model and robot run cycles; the model suggested 10 materials which the robot system then synthesized and analyzed. The cycles were halted after four loops when the model identified the top 10 performing materials of the 286 original samples. Thus, only 40 samples were needed to validate and optimize the model. The authors stress that, as stated in the previous paragraph, BO-guided experiments reduce the time needed to evaluate datasets and optimize materials. In addition, the authors proposed choosing more elements, expanding the abilities of their robot platform, and using multi-objective optimization such as that by Kavalsky *et al.*[57]

5. Discussion

The methods reviewed here show much promise for material discovery to advance electrochemical technologies for energy and chemical applications. Computational methods present the opportunity to explore not-yet-synthesized materials and screen high volumes of data, while HT experimental methods make and test a myriad of samples. Table 4 compares the pros and cons of computational and experimental methods to sum up some of the points we've discussed in this review. Learning from these approaches and setups will hopefully allow more labs and researchers to adopt HT practices and thus find solutions to the roadblocks for implementation at scale. While collecting and summarizing these data, we identified some trends and new focus areas worth capturing and noting in this section.

The distribution of methods reviewed in this article is depicted in Fig. 9a as a bar graph. We can see that most reports

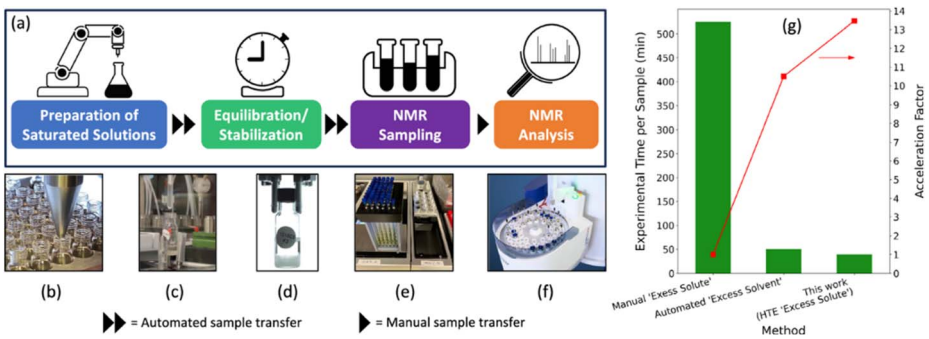

Fig. 8 (a) Schematic representation of the automated HTE system for solubility measurement. The automation process consists of powder (b) and solvent (c) dispensing, (d) saturated sample monitoring, and nuclear magnetic resonance (NMR) sampling (e) and analysis (f). (g) Evaluated experimental time per sample for different solubility measurement methods. Reproduced with permission from ref. 163. Copyright 2024 Springer Nature Ltd.

Table 4 List of pros and cons of computational and experimental HT methods

HT method	Pros	Cons
Experimental	Physical observations & real-world results	Spatial and time limits
	High data reliability	More resource intensive
	Accounts for synthesis conditions	Safety/environmental constraints
Computational	Massive screening (>10^3 materials)	Model accuracy limitations
	Cost-effective and rapid testing	Requires experimental validation
	Safe exploration	Difficulty in capturing synthesizability

conducted HT studies *via* computation, which we expect since it is faster, safer, and less resource-intensive than experiments. There is a significant discrepancy, however, in the material type (Fig. 9b). Of all the publications we discovered and analyzed for this review, over 80% focused on catalysts no matter the reaction. Although responsible for driving the reaction, the catalyst is not the only component of an electrochemical reactor. These percentages in Fig. 9b are only based on the thorough search we conducted in the literature space and thus not representative of the entire field; yet we still suggest that critical components such as membranes, ionomers, and substrates remain underexplored using high-throughput methods although they are necessary in such systems. These components are critical to the long-term operation, durability, and efficiency of electrochemical systems. Many degradation mechanisms that lead to failure and insufficient lifetimes in electrochemical systems are associated with not only the catalyst but also the substrate (or membrane) it is deposited on and/or the ionomer that binds them together, if applicable.[167] The development of polymer informatics platforms could facilitate the discovery of next-generation ionomer and membrane materials that rival or outperform current standards such as Nafion and other PFAS polymers that also present environmental liabilities. Moreover, highly conductive electrolytes provide ion transport but may be corrosive or detrimental to all components in the system in the long term. Although ~12% of the reports investigated electrolytes, most pertain to batteries and not those for fuel cells and electrolyzers. Therefore, this review underscores the need for broader HT efforts that investigate all materials involved in electrochemical reactors to address performance bottlenecks effectively. Nevertheless, we understand that constructing compositional libraries and datasets for materials such as polymers and substrates is more complex than for catalysts. Polymers for ionomers and membranes are not as simple to model as metal catalysts due to their larger size, intricate structures, and heterogeneous nature.[168] These macrostructures generally feature complex arrangements with numerous degrees of freedom, which increases the computational demand of simulations. Like polymers, substrates–materials onto which catalysts are deposited—are also macrostructures and generally heterogeneous. Accurately capturing complex interactions and dynamic behavior of these polymers and substrates with their surroundings requires advanced computational techniques and a considerable number of resources.

Another potentially critical direction involves extending HT methodologies beyond material-level screening to capture device-level performance metrics. Current HT platforms typically evaluate properties such as onset potential, overpotential, or adsorption energy in simplified environments. However, real-world performance is governed by how materials function within integrated systems. Developing modular experimental platforms that can vary multiple components simultaneously—for instance, testing combinations of catalysts, ionomers, and membranes within the same electrochemical cell—would allow for the co-optimization of interdependent variables. Incorporating accelerated stress tests and diagnostics into HT setups could also provide early insights into material degradation

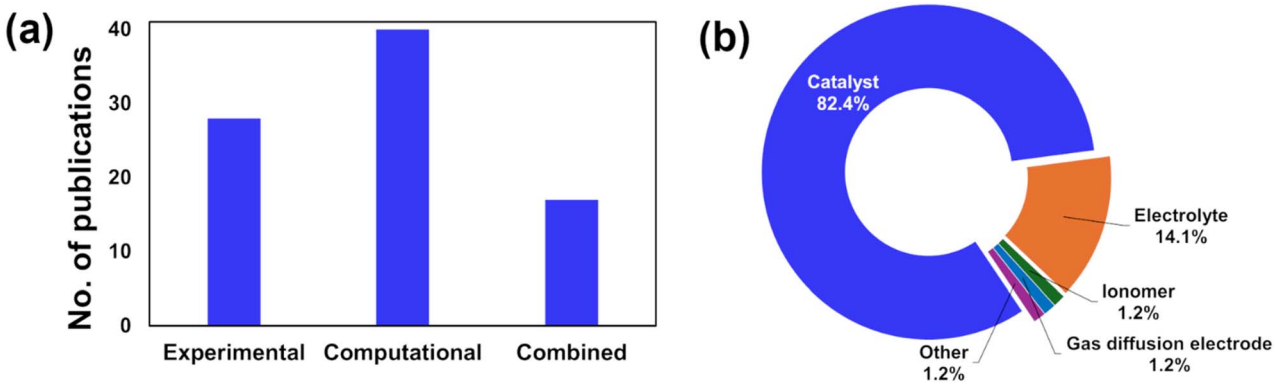

Fig. 9 Analysis of HT literature reviewed. (a) Bar graph depicting the number of publications using either experimental methods, computational methods, or a combination of both for HT material discovery. (b) Pie chart detailing the type of material studied in the literature we reviewed and the percentage of papers that focused on that material. Catalyst materials dominate the HT literature found.

Table 5 Roughly estimated costs of some types of HT equipment for both experimental and computational methods. This list does not cover all instruments that may exist in a HT laboratory. Costs were sourced from vendor quotes and websites

Experimental			Computational	
HT equipment	Method	Average cost (USD)	HT equipment	Average cost (USD)
Scanning flow/droplet cell[169,170]	Electroanalysis	$110 000–$150 000	1-Rack high performance computing cluster with 10 CPU nodes[171–173]	$200 000–$400 000
X-ray diffraction[147]	Characterization	$300 000		
X-ray fluorescence[146,174]	Characterization	$100 000		
Confocal microscopy[175,176]	Characterization	$70 000–$250 000		
Nanoprinter[177]	Synthesis	$350 000	Supercomputing time[178–181]	$0.005–$0.0625 per hour
Automated synthesis platform[182,183]	Synthesis	$70 000–$500 000		
Robotic arm[184,185]	Versatile	$25 000–$100 000		

pathways and lifetime expectations, enabling more predictive screening of materials for industrial relevance.

As mentioned in Section 2.1, many DFT studies successfully utilize activity descriptors, whether ΔG or partial atomic charges, and stability descriptors to screen catalyst materials. While activity and stability are imperative, many of the computational methods reviewed here do not consider the cost, availability, safety, both environmental and personal, and complexity of synthesis when proposing new materials. Some of these suggested materials are dangerous, expensive, and synthetically impractical, which makes their window for scale-up very slim and complicated. In addition, some materials may be sourced from carbon-intensive processes, which defeats the purpose of green technologies and calls for carbon neutrality analysis when discovering and proposing new materials. This issue presents opportunities to discover new descriptors that can screen for these properties, such as hazard diamond ratings or toxicity of precursors, material biodegradability, earth abundance indices, and cost indices of metals (like that used by Kavalsky *et al.*[57]). Jia *et al.* applied cohesive and formation energies as descriptors for ease of synthesis which more researchers can expand on.[63] Integrating life cycle assessment into computational models makes it possible to evaluate the environmental impact and predict the long-term behavior of materials.[186–188] There is also the opportunity to identify and explore other properties and descriptors not named here that are important for a material's feasibility. These descriptors can be extracted from databases, developed using cheminformatics tools, or derived from techno-economic proxies such as precursor cost or process energy intensity. When it comes to experimental methods, more scientists can consider comparing the cost of their suggested material(s) to the state of the art on top of comparing the performance and commenting on the safety of the material(s) they suggest.

In this review, we examined studies that benefit from combining ML and DFT approaches to make their HT screening even more powerful as a tool. However, it is worth mentioning that access to effective and significant computational resources

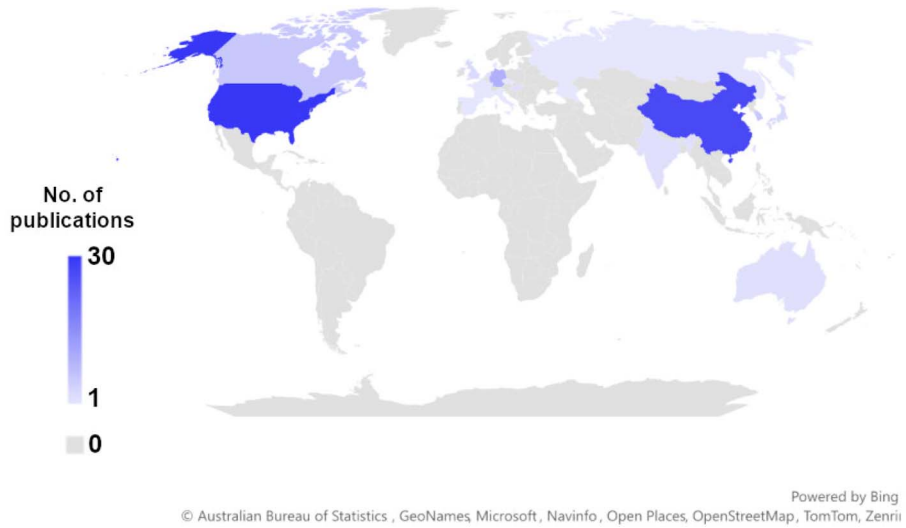

Fig. 10 Heat map highlighting the countries of the authors of the reports evaluated in this review. The darker the shade of blue, the more that country has been associated with a publication *via* authorship. If a country is grey, then no author from the literature we reviewed was affiliated with that country. The map was generated using Microsoft Bing.

applicable to the generation of databases required to train ML models is a challenge for many researchers around the world. The same can be said for experimentation, as fully equipped, functioning labs are expensive to build, let alone automated HT systems. In fact, Table 5 roughly estimates and compares the cost of HT experimental equipment, HT supercomputers, and supercomputing time. The price of a fully functioning HT lab can easily reach $100 000 USD in equipment alone, not considering overhead, utilities, maintenance, *etc.*, to keep it up and running. Access to well-equipped shared facilities such as those found at universities and national labs would remove the burden of procuring such equipment, making HT experiments cheaper. Yet, access to such facilities can be limited to specific users and user rates may apply, which can add to cost over time as more experiments are conducted and more materials are screened.

Going off method costs, we also examined where these HT studies were being conducted. Looking at Fig. 10, we see that most of the HT studies we evaluated here were performed by researchers in only a handful of countries (19). However, the motivation for such studies stems from a global issue. We understand that our review, while thorough, is not exhaustive and can only offer a glimpse of what is occurring in this field. Either way, we in countries with access to these resources can push the envelope and collaborate with those in countries that do not. To democratize participation, future work should prioritize the development of low-cost, open-source datasets, modelling tools and cloud-based simulation platforms that reduce entry barriers. Similarly, the establishment of shared robotic facilities or "HT-as-a-service" centers, where researchers can remotely submit and analyze samples, could dramatically broaden global engagement. Capacity-building programs, research exchanges, and international consortia that foster technology transfer and technical training will be particularly important in regions where energy transitions are most urgently needed. Such collaborations can offer more unique perspectives on HT material discovery, leading to new and improved ideas.

Detailed information on data preprocessing steps and links to datasets were missing in many of the papers that we analyzed in this review. Such information is pertinent as it allows researchers to make informed decisions about comparing model performance and therefore finalize model use for their own studies. Access to datasets and preprocessing steps helps one determine model generalizability and helps improve model interpretability, especially when it comes to "black box" models such as neural networks or ensemble learning models. Furthermore, sharing preprocessing steps allows the research community to (1) validate model performance and results through independent experimentation, leading to more robust models and computational methods and (2) modify and build upon these models and datasets.

We recognize that researchers have already taken steps to make HT computational methods and experimental setups available to everyone. Published studies may include how to obtain the data and links to open-source code (*e.g.*, GitHub). Some authors go so far as to ask readers to comment or build on their results and are open to connecting with other researchers about their work. For uses such as training ML models, finding material properties, or simply comparing results, researchers have created open datasets for people to pull from and/or augment. One example is the Open Catalyst Datasets, which are meant to aid in ML model training.[189,190] This dataset is part of the larger Materials Project which allows researchers to access computed information on known and hypothetical materials.[191] Researchers at the Toyota and the Massachusetts Institute of Technology collaborated to create a cloud platform for sharing polymer electrolyte data.[192] Many other material databases have been designed for similar purposes that scientists continue to add to and use for their research.[193–195] Equally important is the development of standardized experimental formats and reporting guidelines that support machine readability and enable cross-laboratory benchmarking. Practicing open-source research should be continued as it is an imperative tool for materials discovery and is becoming more prevalent among researchers, especially in the fields we discussed here. A coordinated community effort to develop open-access HT datasets, curated with rich metadata including synthesis conditions, characterization protocols, and failure modes, would dramatically expand the reproducibility and generalizability of future research.

6. Outlook

Automated and HT methods for materials discovery can help drive electrochemical technologies toward feasibility at scale. Using computation and experimentation is necessary for identifying and validating materials, and combining both, although difficult, brings about very effective methodologies. Even so, there is room to upgrade models and tweak setups to obtain more accurate results and uncover new chemistries. Quantum computing, for example, could exponentially speed up molecular simulations. Although challenges remain, this technology may enable more accurate modeling of complex electrochemical interfaces.[196] Although we did not discuss it in detail here as it would require an in depth analysis and discussion, scientists have begun developing fully self-driving labs that incorporate artificial intelligence like those established in the Acceleration Consortium at the University of Toronto.[197–200] The Cronin group at the University of Glasgow has explored self-driving labs for material discovery but also from a safety and efficiency perspective to decrease risks for researchers and reduce human error.[201] These systems require robust data infrastructures, including standardized ontologies, seamless interoperability between hardware and software, and feedback mechanisms that enable machine learning models to learn not only from successful trials but also from failed experiments. To realize this vision, future research must also address challenges around system integration, error propagation, and the real-time decision-making capabilities of optimization algorithms such as Bayesian frameworks. With all this in mind, we consider that chemistry-related research toward scalable solutions, and not just for energy applications, may be headed toward fully autonomous laboratories where computation and experimentation work hand-in-hand. The future of HT electrochemical

materials discovery lies in its ability to become more holistic, inclusive, and application-driven. This will require concerted effort not only to advance the tools and techniques themselves, but also to redefine what success looks like in materials discovery—balancing performance with scalability, environmental responsibility, and real-world relevance.

Data availability

No primary research results, software or code have been included, and no new data were generated or analysed as part of this review.

Author contributions

U. N. and J. W. contributed to conceptualization. U. N. wrote the original draft, and K. Y., A. T., J. W. and V. B. contributed additional writing. All authors contributed to reviewing and editing.

Conflicts of interest

There are no conflicts to declare.

Acknowledgements

The authors gratefully acknowledge UL Research Institutes (ULRI) for funding this work. We would also like to acknowledge Hilary Davis and the Library & Research Information Services team at ULRI for helping with finding the relevant literature. Furthermore, we appreciate Pang Siu and the Marketing Operations & Strategy team at ULRI for providing the cover graphics.

References

1 *Global Land and Ocean Average Temperature Anomalies*, **https://www.ncei.noaa.gov/access/monitoring/climate-at-a-glance/global/time-series**, accessed 2024.
2 *Carbon Cycle Gases, Mauna Loa, Hawaii, United States*, **https://gml.noaa.gov/dv/iadv/graph.php?code=MLO&program=ccgg&type=sc**, accessed 2024.
3 *Population*, **https://www.un.org/en/global-issues/population**, accessed 2024.
4 *Bend the Trend – Pathways to a Liveable Planet as Resource Use Spikes*, Nairobi, 2024.
5 *Energy and the Environment Explained: Outlook for Future Emissions*, **https://www.eia.gov/energyexplained/energy-and-the-environment/outlook-for-future-emissions.php**, accessed 2024.
6 *Global Non-CO_2 Greenhouse Gas Emission Projections & Mitigation: 2015–2050*, Washington DC, 2019.
7 S. Fawzy, A. I. Osman, J. Doran and D. W. Rooney, *Environ. Chem. Lett.*, 2020, **18**, 2069–2094.
8 D. Panepinto, V. A. Riggio and M. Zanetti, *Int. J. Environ. Res. Public Health*, 2021, **18**, 6767.
9 H. Nami, O. B. Rizvandi, C. Chatzichristodoulou, P. V. Hendriksen and H. L. Frandsen, *Energy Convers. Manage.*, 2022, **269**, 116162.
10 R. M. Darling, *Curr. Opin. Chem. Eng.*, 2022, **37**, 100855.
11 T. Terlouw, C. Bauer, R. McKenna and M. Mazzotti, *Energy Environ. Sci.*, 2022, **15**, 3583–3602.
12 S. Verma, B. Kim, H. R. Jhong, S. Ma and P. J. Kenis, *ChemSusChem*, 2016, **9**, 1972–1979.
13 M. Jouny, W. Luc and F. Jiao, *Ind. Eng. Chem. Res.*, 2018, **57**, 2165–2177.
14 A. G. Wills, S. Charvet, C. Battilocchio, C. C. Scarborough, K. M. P. Wheelhouse, D. L. Poole, N. Carson and J. C. Vantourout, *Org. Process Res. Dev.*, 2021, **25**, 2587–2600.
15 T. H. Muster, A. Trinchi, T. A. Markley, D. Lau, P. Martin, A. Bradbury, A. Bendavid and S. Dligatch, *Electrochim. Acta*, 2011, **56**, 9679–9699.
16 A. Jain, G. Hautier, C. J. Moore, S. Ping Ong, C. C. Fischer, T. Mueller, K. A. Persson and G. Ceder, *Comput. Mater. Sci.*, 2011, **50**, 2295–2310.
17 R. Cai, K. Yang, X. Wang, M. Rukh, A. S. Bosari, E. Giavedoni, A. Pierce, L. Brody, W. Tang, P. R. Westmoreland and F. Li, *Energy Environ. Sci.*, 2024, **17**, 6279–6290.
18 Y. Ding, L. Tong, X. Liu, Y. Liu and Y. Zhao, *Energy Environ. Mater.*, 2025, e70041.
19 W. Yi Wang, J. Li, W. Liu and Z.-K. Liu, *Comput. Mater. Sci.*, 2019, **158**, 42–48.
20 A. Jain, Y. Shin and K. A. Persson, *Nat. Rev. Mater.*, 2016, **1**, 15004.
21 S. Curtarolo, G. L. W. Hart, M. B. Nardelli, N. Mingo, S. Sanvito and O. Levy, *Nat. Mater.*, 2013, **12**, 191–201.
22 A. J. Cohen, P. Mori-Sánchez and W. Yang, *Chem. Rev.*, 2012, **112**, 289–320.
23 A. J. Freeman and E. Wimmer, *Annu. Rev. Mater. Res.*, 1995, **25**, 7–36.
24 R. G. Parr, *Density Functional Theory of Atoms and Molecules*, ed. K. Fukui and B. Pullman, Springer Netherlands, 1980, pp. 5–15.
25 W. Kohn and L. J. Sham, *Phys. Rev.*, 1965, **140**, A1133–A1138.
26 J. Wellendorff, T. L. Silbaugh, D. Garcia-Pintos, J. K. Nørskov, T. Bligaard, F. Studt and C. T. Campbell, *Surf. Sci.*, 2015, **640**, 36–44.
27 J. Wellendorff, K. T. Lundgaard, A. Møgelhøj, V. Petzold, D. D. Landis, J. K. Nørskov, T. Bligaard and K. W. Jacobsen, *Phys. Rev. B:Condens. Matter Mater. Phys.*, 2012, **85**, 235149.
28 K. Yang and B. Yang, *Faraday Discuss.*, 2021, **229**, 50–61.
29 A. H. Cheng, C. T. Ser, M. Skreta, A. Guzmán-Cordero, L. Thiede, A. Burger, A. Aldossary, S. X. Leong, S. Pablo-García, F. Strieth-Kalthoff and A. Aspuru-Guzik, *Faraday Discuss.*, 2024, **256**, 10–60.
30 R. Car, *Quant. Struct.-Act. Relat.*, 2002, **21**, 97–104.
31 J. Cheng, X. Liu, J. VandeVondele, M. Sulpizi and M. Sprik, *Acc. Chem. Res.*, 2014, **47**, 3522–3529.
32 S. P. Ong, O. Andreussi, Y. Wu, N. Marzari and G. Ceder, *Chem. Mater.*, 2011, **23**, 2979–2986.

33 H.-J. Chun, V. Apaja, A. Clayborne, K. Honkala and J. Greeley, *ACS Catal.*, 2017, **7**, 3869–3882.
34 C. F. Dickens, J. H. Montoya, A. R. Kulkarni, M. Bajdich and J. K. Nørskov, *Surf. Sci.*, 2019, **681**, 122–129.
35 K. Yang, J. Zaffran and B. Yang, *Phys. Chem. Chem. Phys.*, 2020, **22**, 890–895.
36 J. K. Nørskov, J. Rossmeisl, A. Logadottir, L. Lindqvist, J. R. Kitchin, T. Bligaard and H. Jónsson, *J. Phys. Chem. B*, 2004, **108**, 17886–17892.
37 A. G. Yohannes, C. Lee, P. Talebi, D. H. Mok, M. Karamad, S. Back and S. Siahrostami, *ACS Catal.*, 2023, **13**, 9007–9017.
38 X. F. Ma, Z. Li, L. E. K. Achenie and H. L. Xin, *J. Phys. Chem. Lett.*, 2015, **6**, 3528–3533.
39 S. Wang, L. Li, J. Li, C. Z. Yuan, Y. Kang, K. S. Hui, J. T. Zhang, F. Bin, X. Fan, F. M. Chen and K. N. Hui, *J. Phys. Chem. C*, 2021, **125**, 7155–7165.
40 S. Ananthaneni and R. B. Rankin, *J. Comput. Chem.*, 2020, **41**, 1384–1394.
41 T. Yang, J. Zhou, T. T. Song, L. Shen, Y. P. Feng and M. Yang, *ACS Energy Lett.*, 2020, **5**, 2313–2321.
42 N. Ran, B. Sun, W. J. Qiu, E. H. Song, T. W. Chen and J. J. Liu, *J. Phys. Chem. Lett.*, 2021, **12**, 2102–2111.
43 J. N. Zheng, X. Sun, C. L. Qu, Y. L. Yan, Z. H. Yao, S. W. Deng, X. Zhong, G. L. Zhuang, Z. Z. Wei and J. G. Wang, *J. Phys. Chem. C*, 2020, **124**, 13695–13705.
44 M. Umer, S. Umer, M. Zafari, M. R. Ha, R. Anand, A. Hajibabaei, A. Abbas, G. Lee and K. S. Kim, *J. Mater. Chem. A*, 2022, **10**, 6679–6689.
45 C. W. Xiao, R. J. Sa, Z. J. Ma, Z. T. Cui, W. Du, X. Q. Sun, Q. H. Li and H. L. Deng, *Int. J. Hydrogen Energy*, 2021, **46**, 10337–10345.
46 L. Ge, H. Yuan, Y. X. Min, L. Li, S. Q. Chen, L. Xu and W. A. Goddard, *J. Phys. Chem. Lett.*, 2020, **11**, 869–876.
47 R. X. Xu, T. T. Bo, S. Q. Cao, N. Mu, Y. Y. Liu, M. Y. Chen and W. Zhou, *J. Mater. Chem. A*, 2022, **10**, 21315–21326.
48 X. Song, Z. H. Li, L. Sheng and N. Xiao, *Appl. Surf. Sci.*, 2023, **639**, 158225.
49 J. W. Zhang, P. J. Hu and H. F. Wang, *J. Phys. Chem. C*, 2020, **124**, 10483–10494.
50 X. Zhang, K. P. Li, B. Wen, J. Ma and D. F. Diao, *Chin. Chem. Lett.*, 2023, **34**(5), 107833.
51 M. V. Jyothirmai, R. Dantuluri, P. Sinha, B. M. Abraham and J. K. Singh, *ACS Appl. Mater. Interfaces*, 2024, **16**, 12437–12445.
52 B. M. Abraham, P. Sinha, P. Halder and J. K. Singh, *J. Mater. Chem. A*, 2023, **11**, 8091–8100.
53 H. X. Liang, P. F. Liu, M. Xu, H. T. Li and E. Asselin, *Int. J. Quantum Chem.*, 2023, **123**(6), e27055.
54 L. Yang, J. K. Fan and W. H. Zhu, *Carbon*, 2024, **222**, 119006.
55 X. Y. Li, R. Chiong, Z. Y. Hu and A. J. Page, *J. Phys. Chem. Lett.*, 2021, **12**, 7305–7311.
56 X. N. Mao, L. Wang, Y. F. Xu, P. J. Wang, Y. Y. Li and J. J. Zhao, *npj Comput. Mater.*, 2021, **7**(1), 46.
57 L. Kavalsky, V. I. Hegde, B. Meredig and V. Viswanathan, *Digital Discovery*, 2024, **3**, 999–1010.
58 Z. W. Chen, Z. L. Lu, L. X. Chen, M. Jiang, D. C. Chen and C. V. Singh, *Chem Catal.*, 2021, **1**, 183–195.
59 L. Xu, L. M. Yang and E. Ganz, *ACS Appl. Mater. Interfaces*, 2021, **13**, 14091–14101.
60 S. Back, K. Tran and Z. W. Ulissi, *ACS Appl. Mater. Interfaces*, 2020, **12**, 38256–38265.
61 H. Park, Y. Kim, S. Choi and H. J. Kim, *J. Energy Chem.*, 2024, **91**, 645–655.
62 R. Jacobs, J. Liu, H. Abernathy and D. Morgan, *Adv. Energy Mater.*, 2024, **14**(12), 2303684.
63 J. J. Jia, S. Q. Wei, Q. H. Cai and J. X. Zhao, *J. Colloid Interface Sci.*, 2021, **600**, 711–718.
64 C. Wang, B. Wang, C. H. Wang, Z. P. Chang, M. Q. Yang and R. Z. Wang, *ACS Appl. Mater. Interfaces*, 2024, **16**, 16050–16061.
65 X. Jia and H. Li, *J. Mater. Chem. A*, 2024, **12**, 12487–12500.
66 M. D. Bhatt, G. Lee and J. S. Lee, *Energy Fuels*, 2017, **31**, 1874–1881.
67 A. Cho, B. J. Park and J. W. Han, *Front. Chem.*, 2022, **10**, 873609.
68 M. C. Tsai, J. Rick, W. N. Su and B. J. Hwang, *Mol. Syst. Des. Eng.*, 2017, **2**, 449–456.
69 H. Tran, K. H. Shen, S. Shukla, H. K. Kwon and R. Ramprasad, *J. Phys. Chem. C*, 2023, **127**(2), 977–986.
70 O. Borodin, M. Olguin, C. E. Spear, K. W. Leiter and J. Knap, *Nanotechnology*, 2015, **26**(35), 354003.
71 D. Barter, E. W. C. Spotte-Smith, N. S. Redkar, A. Khanwale, S. Dwaraknath, K. A. Persson and S. M. Blau, *Digital Discovery*, 2023, **2**, 123–137.
72 L. Cheng, R. S. Assary, X. H. Qu, A. Jain, S. P. Ong, N. N. Rajput, K. Persson and L. A. Curtiss, *J. Phys. Chem. Lett.*, 2015, **6**, 283–291.
73 S. Baker, J. Pagotto, T. T. Duignan and A. J. Page, *J. Phys. Chem. Lett.*, 2023, **14**, 9508–9515.
74 Z. Yang, W. Y. Ye, X. Lei, D. Schweigert, H.-K. Kwon and A. Khajeh, *arXiv*, 2024, preprint, arXiv:2312.06470, DOI: **10.48550/arXiv.2312.06470**.
75 A. Khajeh, X. Lei, W. Ye, Z. Yang, D. Schweigert and H.-K. Kwon, *arXiv*, 2023, preprint, arXiv:2312.04013, DOI: **10.48550/arXiv.2312.04013**.
76 S. A. Tawfik, J. Berk, T. R. Walsh, S. Rana and S. Venkatesh, *J. Phys. Chem. C*, 2025, **129**, 6148–6156.
77 S. R. Xie, S. J. Honrao and J. W. Lawson, *Chem. Mater.*, 2024, **36**, 9320–9329.
78 J. Baek, Q. Jin, N. S. Johnson, Y. Jiang, R. Ning, A. Mehta, S. Siahrostami and X. L. Zheng, *Nat. Commun.*, 2022, **13**(1), 7685.
79 Z. Song, L. Fan, S. Lu, Q. Zhou, C. Ling and J. Wang, *arXiv*, 2024, preprint, arXiv:2405.18891, DOI: **10.48550/arXiv.2405.18891**.
80 J. Y. Peng, L. Giordano, T. C. Davenport and Y. Shao-Horn, *Chem. Mater.*, 2022, **34**, 7774–7787.
81 S. Chibani and F.-X. Coudert, *APL Mater.*, 2020, **8**(8), 080701.
82 Z. Song, L. Fan, S. Lu, C. Ling, Q. Zhou and J. Wang, *Nat. Commun.*, 2025, **16**, 1053.
83 S. Li and A. S. Barnard, *Chem. Mater.*, 2022, **34**, 4964–4974.
84 M. Alverson, S. G. Baird, R. Murdock, S.-H. Ho, J. Johnson and T. D. Sparks, *Digital Discovery*, 2024, **3**, 62–80.

85 K. Bang, J. Kim, D. Hong, D. Kim and S. Soo Han, *J. Mater. Chem. A*, 2024, **12**, 6004–6013.
86 K. Li, B. DeCost, K. Choudhary, M. Greenwood and J. Hattrick-Simpers, *npj Comput. Mater.*, 2023, **9**, 55.
87 L. Himanen, A. Geurts, A. S. Foster and P. Rinke, *Adv. Sci.*, 2019, **6**, 1900808.
88 Z. Levell, J. Le, S. Yu, R. Wang, S. Ethirajan, R. Rana, A. Kulkarni, J. Resasco, D. Lu, J. Cheng and Y. Liu, *Chem. Rev.*, 2024, **124**(4), 8620–8656.
89 *MGI Homepage | Materials Genome Initiative*, **https://www.mgi.gov/**, accessed June 19, 2025.
90 S. P. Stier, C. Kreisbeck, H. Ihssen, M. A. Popp, J. Hauch, K. Malek, M. Reynaud, T. p. m. Goumans, J. Carlsson, I. Todorov, L. Gold, A. Räder, W. Wenzel, S. T. Bandesha, P. Jacques, F. Garcia-Moreno, O. Arcelus, P. Friederich, S. Clark, M. Maglione, A. Laukkanen, I. E. Castelli, J. Carrasco, M. C. Cabanas, H. S. Stein, O. Ozcan, D. Elbert, K. Reuter, C. Scheurer, M. Demura, S. S. Han, T. Vegge, S. Nakamae, M. Fabrizio and M. Kozdras, *Adv. Mater.*, 2024, **36**, 2407791.
91 *The Novel Materials Discovery Laboratory | NoMaD | Projekt | Fact Sheet | H2020*, **https://cordis.europa.eu/project/id/676580**, accessed June 9, 2025.
92 K. Shahzad, A. I. Mardare and A. W. Hassel, *Sci. Technol. Adv. Mater.:Methods*, 2024, **4**, 2292486.
93 M. Chatenet, B. G. Pollet, D. R. Dekel, F. Dionigi, J. Deseure, P. Millet, R. D. Braatz, M. Z. Bazant, M. Eikerling, I. Staffell, P. Balcombe, Y. Shao-Horn and H. Schäfer, *Chem. Soc. Rev.*, 2022, **51**, 4583–4762.
94 K. Scott, in *Electrochemical Methods for Hydrogen Production*, ed. K. Scott, The Royal Society of Chemistry, 2019.
95 H.-R. M. Jhong, S. Ma and P. J. A. Kenis, *Curr. Opin. Chem. Eng.*, 2013, **2**, 191–199.
96 X. Zhao, G. Hu, G.-F. Chen, H. Zhang, S. Zhang and H. Wang, *Adv. Mater.*, 2021, **33**, 2007650.
97 J. G. Chen, R. M. Crooks, L. C. Seefeldt, K. L. Bren, R. M. Bullock, M. Y. Darensbourg, P. L. Holland, B. Hoffman, M. J. Janik, A. K. Jones, M. G. Kanatzidis, P. King, K. M. Lancaster, S. V. Lymar, P. Pfromm, W. F. Schneider and R. R. Schrock, *Science*, 2018, **360**, eaar6611.
98 L. Kavalsky, *Autocat*.
99 *PFAS Explained*.
100 *Per- and Polyfluoroalkyl Substances (PFAS)*.
101 J. L. Hitt, Y. G. C. Li, S. S. Tao, Z. F. Yan, Y. Gao, S. J. L. Billinge and T. E. Mallouk, *Nat. Commun.*, 2021, **12**(1), 1114.
102 F. D. Mayer, P. Hosseini-Benhangi, C. M. Sánchez-Sánchez, E. Asselin and E. L. Gyenge, *Commun. Chem.*, 2020, **3**(1), 155.
103 J. F. He, K. E. Dettelbach, D. A. Salvatore, T. F. Li and C. P. Berlinguette, *Angew. Chem., Int. Ed.*, 2017, **56**, 6068–6072.
104 Y. Lai, R. J. R. Jones, Y. Wang, L. Zhou and J. M. Gregoire, *ACS Comb. Sci.*, 2019, **21**, 692–704.
105 C. Zhang, Y. T. Luo, J. Y. Tan, Q. M. Yu, F. N. Yang, Z. Y. Zhang, L. S. Yang, H. M. Cheng and B. L. Liu, *Nat. Commun.*, 2020, **11**(1), 3724.
106 P. Zou, L. J. Song, W. Xu, M. Gao, V. Zadorozhnyy, J. T. Huo and J. Q. Wang, *J. Alloys Compd.*, 2023, **960**, 170656.
107 X. Z. Liu, P. Zou, L. J. Song, B. W. Zang, B. N. Yao, W. Xu, F. S. Li, J. Schroers, J. T. Huo and J. Q. Wang, *ACS Catal.*, 2022, **12**, 3789–3796.
108 S. Schumacher, S. Baha, A. Savan, C. Andronescu and A. Ludwig, *J. Mater. Chem. A*, 2022, **10**, 9981–9987.
109 X. Wang, I. A. Cechanaviciute, L. Banko, S. Pokharel, T. Quast, A. Ludwig, O. Krysiak and W. Schuhmann, *Adv. Funct. Mater.*, 2024, **34**, 2400180.
110 F. M. Sapountzi, M. Lavorenti, W. Vrijburg, S. Dimitriadou, B. Tyburska-Pueschel, P. Thüne, H. Niemantsverdriet, T. V. Pfeiffer and M. N. Tsampas, *Catalysts*, 2022, **12**, 1343.
111 K. J. Jenewein, G. D. Akkoc, A. Kormányos and S. Cherevko, *Chem Catal.*, 2022, **2**, 2778–2794.
112 J. M. Gregoire, C. X. Xiang, X. N. Liu, M. Marcin and J. Jin, *Rev. Sci. Instrum.*, 2013, **84**(2), 024102.
113 J. M. Gregoire, C. Xiang, S. Mitrovic, X. Liu, M. Marcin, E. W. Cornell, J. Fan and J. Jin, *J. Electrochem. Soc.*, 2013, **160**, F337–F342.
114 J. A. Haber, C. X. Xiang, D. Guevarra, S. H. Jung, J. Jin and J. M. Gregoire, *Chemelectrochem*, 2014, **1**, 524–528.
115 J. A. Haber, D. Guevarra, S. H. Jung, J. Jin and J. M. Gregoire, *Chemelectrochem*, 2014, **1**, 1613–1617.
116 L. Zhou, A. Shinde, M. C. Chang, R. B. van Dover, M. O. Thompson and J. M. Gregoire, *J. Mater. Chem. A*, 2023, **11**, 25262–25267.
117 Y. Okazaki, Y. Tokudome, S. Yagi and I. Yamada, *Mater. Trans.*, 2023, **64**, 2082–2087.
118 C. Schwanke, H. S. Stein, L. Xi, K. Sliozberg, W. Schuhmann, A. Ludwig and K. M. Lange, *Sci. Rep.*, 2017, **7**, 44192.
119 Y. J. Li, H. Wu, J. F. Zhang, Q. Lu, X. P. Han, X. R. Zheng, Y. D. Deng and W. B. Hu, *J. Mater. Chem. A*, 2023, **11**, 10267–10276.
120 A. K. Schuppert, A. A. Topalov, I. Katsounaros, S. O. Klemm and K. J. J. Mayrhofer, *J. Electrochem. Soc.*, 2012, **159**, F670–F675.
121 Y. G. Yao, Z. N. Huang, T. Y. Li, H. Wang, Y. F. Liu, H. S. Stein, Y. M. Mao, J. L. Gao, M. L. Jiao, Q. Dong, J. Q. Dai, P. F. Xie, H. Xie, S. D. Lacey, I. Takeuchi, J. M. Gregoire, R. Z. Jiang, C. Wang, A. D. Taylor, R. Shahbazian-Yassar and L. B. Hu, *Proc. Natl. Acad. Sci. U. S. A.*, 2020, **117**, 6316–6322.
122 I. Reichmann, V. Lloret, K. Ehelebe, P. Lauf, K. Jenewein, K. J. J. Mayrhofer and S. Cherevko, *ACS Meas. Sci. Au*, 2024, **4**(5), 515–527.
123 O. A. Krysiak, S. Schumacher, A. Savan, W. Schuhmann, A. Ludwig and C. Andronescu, *Nano Res.*, 2022, **15**, 4780–4784.
124 R. Becker, K. Weber, T. V. Pfeiffer, J. van Kranendonk and K. J. Schouten, *Catalysts*, 2020, **10**, 1165.
125 M. Minichová, C. Van Pham, B. Xiao, A. Savan, A. Hutzler, A. Körner, I. Khalakhan, M. G. Rodríguez, I. Mangoufis-

Giasin, V. Briega-Martos, A. Kormányos, I. Katsounaros, K. J. J. Mayrhofer, A. Ludwig, S. Thiele and S. Cherevko, *Electrochim. Acta*, 2023, **444**, 142032.
126 R. Liu and E. S. Smotkin, *J. Electroanal. Chem.*, 2002, **535**, 49–55.
127 R. J. R. Jones, Y. Lai, D. Guevarra, K. Kan, J. A. Haber and J. M. Gregoire, *Digital Discovery*, 2024, **3**, 1144–1149.
128 J.-P. Grote, A. R. Zeradjanin, S. Cherevko and K. J. J. Mayrhofer, *Rev. Sci. Instrum.*, 2014, **85**(10), 104101.
129 K. J. Jenewein, S. Thienhaus, A. Kormányos, A. Ludwig and S. Cherevko, *Chem. Sci.*, 2022, **13**, 13774–13781.
130 H. Joress, B. L. DeCost, S. Sarker, T. M. Braun, S. Jilani, R. Smith, L. Ward, K. J. Laws, A. Mehta and J. R. Hattrick-Simpers, *ACS Comb. Sci.*, 2020, **22**, 330–338.
131 K. K. Rao, L. Zhou, Y. C. Lai, M. H. Richter, X. Li, Y. B. Lu, J. Yano, J. M. Gregoire and M. Bajdich, *J. Mater. Chem. A*, 2023, **11**, 5166–5178.
132 K. Kan, D. Guevarra, L. Zhou, R. J. R. Jones, Y. Lai, M. Richter and J. M. Gregoire, *ChemCatChem*, 2024, **16**, e202301300.
133 A. A. Topalov, I. Katsounaros, M. Auinger, S. Cherevko, J. C. Meier, S. O. Klemm and K. J. J. Mayrhofer, *Angew. Chem., Int. Ed.*, 2012, **51**, 12613–12615.
134 M. Nowak, R. Gutkowski, J. Junqueira, W. Schuhmann and A. Ludwig, *Z. Phys. Chem.*, 2020, **234**, 835–845.
135 M. Raicopol, B. Bălănucă, K. Sliozberg, B. Schlüter, S. A. Gârea, N. Chira, W. Schuhmann and C. Andronescu, *Corros. Sci.*, 2015, **100**, 386–395.
136 S. O. Klemm, A. A. Topalov, C. A. Laska and K. J. J. Mayrhofer, *Electrochem. Commun.*, 2011, **13**, 1533–1535.
137 K. Sliozberg, D. Schäfer, T. Erichsen, R. Meyer, C. Khare, A. Ludwig and W. Schuhmann, *ChemSusChem*, 2015, **8**, 1270–1278.
138 B. C. Chan, R. Liu, K. Jambunathan, H. Zhang, G. Chen, T. E. Mallouk and E. S. Smotkin, *J. Electrochem. Soc.*, 2005, **152**, A594.
139 E. S. Smotkin, J. Jiang, A. Nayar and R. Liu, *Appl. Surf. Sci.*, 2006, **252**, 2573–2579.
140 E. S. Smotkin, *US Pat.*, US6692856B2, 2001.
141 B. Cantor and R. W. Cahn, *Acta Metall.*, 1976, **24**, 845–852.
142 N. Vervoort, K. Goossens, M. Baeten and Q. Chen, *Anal. Sci. Adv.*, 2021, **2**, 109–127.
143 I. G. Clayson, D. Hewitt, M. Hutereau, T. Pope and B. Slater, *Adv. Mater.*, 2020, **32**, 2002780.
144 F. Jia, Y. Ma and R. Ahmad, *Int. J. Adv. Manuf. Technol.*, 2024, **131**, 1039–1057.
145 *Fourier Sample Changer*, **https://www.bruker.com/en/products-and-solutions/mr/nmr/nmr-automation.html**, accessed June 6, 2025.
146 *M4 TORNADO*, **https://www.bruker.com/en/products-and-solutions/elemental-analyzers/micro-xrf-spectrometers/m4-tornado.html**, accessed June 6, 2025.
147 *D8 DISCOVER*, **https://www.bruker.com/en/products-and-solutions/diffractometers-and-x-ray-microscopes/x-ray-diffractometers/d8-discover-family/d8-discover.html**, accessed June 6, 2025.
148 *ASAP 2460 & 2425*, **https://micromeritics.com/products/asap-2460-2425/**, accessed June 6, 2025.
149 N. J. Szymanski, C. J. Bartel, Y. Zeng, M. Diallo, H. Kim and G. Ceder, *npj Comput. Mater.*, 2023, **9**, 31.
150 G. T. Hai, X. D. Xue, S. H. Feng, Y. W. Ma and X. B. Huang, *ACS Catal.*, 2022, **12**, 15271–15281.
151 J. Greeley, T. F. Jaramillo, J. Bonde, I. Chorkendorff and J. K. Nørskov, *Nat. Mater.*, 2006, **5**, 909–913.
152 D. Q. Guan, J. Zhou, Y. C. Huang, C. L. Dong, J. Q. Wang, W. Zhou and Z. P. Shao, *Nat. Commun.*, 2019, **10**, 3755.
153 M. Kodera and K. Sayama, *Digital Discovery*, 2023, **2**, 1683–1687.
154 W. Zhou, L. Yang, X. Wang, W. L. Zhao, J. X. Yang, D. Zhai, L. Sun and W. Q. Deng, *JACS Au*, 2021, **1**, 1497–1505.
155 S. G. Hari Kumar, C. Bozal-Ginesta, N. Wang, J. Abed, C. H. Shan, Z. Yao and A. Aspuru-Guzik, *Chem. Sci.*, 2024, **15**, 10556–10570.
156 M. R. Karim, M. Ferrandon, S. Medina, E. Sture, N. Kariuki, D. J. Myers, E. F. Holby, P. Zelenay and T. Ahmed, *ACS Appl. Energy Mater.*, 2020, **3**, 9083–9088.
157 X. Zhao, Q. Yin, X. N. Mao, C. Cheng, L. Zhang, L. Wang, T. F. Liu, Y. Y. Li and Y. G. Li, *Nat. Commun.*, 2022, **13**(1), 2721.
158 Y. Y. Pan, X. Y. Shan, F. R. Cai, H. Gao, J. N. Xu and M. Zhou, *Angew. Chem., Int. Ed.*, 2024, **63**(37), e202407116.
159 M. Sarwar, J. L. Gavartin, A. Martinez Bonastre, S. Garcia Lopez, D. Thompsett, S. C. Ball, A. Krzystala, G. Goldbeck and S. A. French, *Phys. Chem. Chem. Phys.*, 2020, **22**, 5902–5914.
160 Z. Luo, X. Hu, Y. Zhou, Y. Ding, W. Zhang, T. Li and M. Liu, *Adv. Mater.*, 2024, **36**, 2311159.
161 C. Chen, D. T. Nguyen, S. J. Lee, N. A. Baker, A. S. Karakoti, L. Lauw, C. Owen, K. T. Mueller, B. A. Bilodeau, V. Murugesan and M. Troyer, *J. Am. Chem. Soc.*, 2024, **146**, 20009–20018.
162 A. Narayanan Krishnamoorthy, C. Wölke, D. Diddens, M. Maiti, Y. Mabrouk, P. Yan, M. Grünebaum, M. Winter, A. Heuer and I. Cekic-Laskovic, *Chemistrymethods*, 2022, **2**(9), e202200008.
163 J. Noh, H. A. Doan, H. Job, L. A. Robertson, L. Zhang, R. S. Assary, K. Mueller, V. Murugesan and Y. A. Liang, *Nat. Commun.*, 2024, **15**(1), 2757.
164 L. Shen, Z. Wang, S. Xu, H. M. Law, Y. Zhou and F. Ciucci, *Nat. Commun.*, 2025, **16**, 3687.
165 S. Muy, J. Voss, R. Schlem, R. Koerver, S. J. Sedlmaier, F. Maglia, P. Lamp, W. G. Zeier and Y. Shao-Horn, *iScience*, 2019, **16**, 270–282.
166 C. J. Bartel, *J. Mater. Sci.*, 2022, **57**, 10475–10498.
167 U. O. Nwabara, E. R. Cofell, S. Verma, E. Negro and P. J. A. Kenis, *ChemSusChem*, 2020, **13**, 855–875.
168 N. Yao, X. Chen, Z.-H. Fu and Q. Zhang, *Chem. Rev.*, 2022, **122**, 10970–11021.
169 *ac/dc-SDS – M470*, **https://www.biologic.net/products/ac-dc-sdc-m470/**, accessed June 9, 2025.
170 *SDC Scanning Droplet Cell | Princeton Applied Research*, **https://www.ameteksi.com/products/**

scanningelectrochemicalsystems/sdc-scanning-droplet-cell, accessed June 9, 2025.
171 *High Performance Computing (HPC) Solutions | #1 Supercomputer Provider Globally | Lenovo US*, https://www.lenovo.com/us/en/servers-storage/solutions/hpc/, accessed June 19, 2025.
172 *High Performance Computing (HPC) & AI Innovation Lab | Dell USA*, https://www.dell.com/en-us/lp/dt/hpc-ai-innovation-lab, accessed June 19, 2025.
173 *High-performance Computing Power from Anywhere*, https://www.hp.com/us-en/workstations/learning-hub/high-performance-computing-power.html, accessed June 19, 2025.
174 *S8 TIGER*, https://www.bruker.com/en/products-and-solutions/elemental-analyzers/xrf-spectrometers/s8-tiger.html, accessed June 9, 2025.
175 *3D Surface Profiler – VK-X3000 series | KEYENCE America*, https://www.keyence.com/products/microscope/laser-microscope/vk-x3000/, accessed June 9, 2025.
176 *MSE PRO Confocal Microscope with 200 × 200 mm Table Size, 10 kg Load capacity*, https://www.msesupplies.com/products/mse-pro-confocal-microscope-with-200x200-mm-table-size-10-kg-load-capacity, accessed June 9, 2025.
177 *VSPARTICLE*, https://vsparticle.com/, accessed June 9, 2025.
178 *Rates – SCG*, https://login.scg.stanford.edu/rates/, accessed June 5, 2025.
179 *Great Lakes Service Rates*, https://its.umich.edu/advanced-research-computing/high-performance-computing/great-lakes/rates, accessed June 5, 2025.
180 *High-performance computing (HPC) | HMS IT*, https://it.hms.harvard.edu/service/high-performance-computing-hpc, accessed June 5, 2025.
181 *Rates | HPC Center*, https://www.hpc.caltech.edu/rates, accessed June 5, 2025.
182 *Life Science Tools | Unchained Labs*, https://www.unchainedlabs.com/, accessed June 9, 2025.
183 *Leading edge Solutions for Lab Automation & Digitalization*, https://www.chemspeed.com/, accessed June 9, 2025.
184 *Robot machine price*, https://standardbots.com/blog/robot-machine-price-how-much-do-they-cost, accessed June 9, 2025.
185 *UR Series*, https://www.universal-robots.com/, accessed June 9, 2025.
186 A. Fong, A. McPherson, M. Rossi and K. Rajan, *MRS Energy Sustain.*, 2024, **12**, 112–120.
187 A. Larrabide, I. Rey and E. Lizundia, *Adv. Energy Sustainability Res.*, 2022, **3**, 2200079.
188 L. Tang, P. Leung, Q. Xu and C. Flox, *ChemElectroChem*, 2024, **11**, e202400024.
189 L. Chanussot, A. Das, S. Goyal, T. Lavril, M. Shuaibi, M. Riviere, K. Tran, J. Heras-Domingo, C. Ho, W. Hu, A. Palizhati, A. Sriram, B. Wood, J. Yoon, D. Parikh, C. L. Zitnick and Z. Ulissi, *ACS Catal.*, 2021, **11**, 6059–6072.
190 R. Tran, J. Lan, M. Shuaibi, B. M. Wood, S. Goyal, A. Das, J. Heras-Domingo, A. Kolluru, A. Rizvi, N. Shoghi, A. Sriram, F. Therrien, J. Abed, O. Voznyy, E. H. Sargent, Z. Ulissi and C. L. Zitnick, *ACS Catal.*, 2023, **13**, 3066–3084.
191 A. Jain, S. P. Ong, G. Hautier, W. Chen, W. D. Richards, S. Dacek, S. Cholia, D. Gunter, D. Skinner, G. Ceder and K. A. Persson, *APL Mater.*, 2013, **1**(1), 011002.
192 T. Xie, H.-K. Kwon, D. Schweigert, S. Gong, A. France-Lanord, A. Khajeh, E. Crabb, M. Puzon, C. Fajardo, W. Powelson, Y. Shao-Horn and J. C. Grossman, *APL Mach. Learn.*, 2023, **1**(4), 046108.
193 G. Bergerhoff and I. D. Brown, in *Crystallographic Databases*, ed. F. H. Allen, G. Bergerhoff and R. Sievers, International Union of Crystallography, Chester, England, 1987.
194 S. Kirklin, J. E. Saal, B. Meredig, A. Thompson, J. W. Doak, M. Aykol, S. Rühl and C. Wolverton, *npj Comput. Mater.*, 2015, **1**, 15010.
195 J. E. Saal, S. Kirklin, M. Aykol, B. Meredig and C. Wolverton, *JOM*, 2013, **65**, 1501–1509.
196 S. Hariharan, S. Kinge and L. Visscher, *J. Chem. Inf. Model.*, 2025, **65**, 472–511.
197 G. Tom, S. P. Schmid, S. G. Baird, Y. Cao, K. Darvish, H. Hao, S. Lo, S. Pablo-García, E. M. Rajaonson, M. Skreta, N. Yoshikawa, S. Corapi, G. D. Akkoc, F. Strieth-Kalthoff, M. Seifrid and A. Aspuru-Guzik, *Chem. Rev.*, 2024, **124**, 9633–9732.
198 Y. Bai, L. Wilbraham, B. J. Slater, M. A. Zwijnenburg, R. S. Sprick and A. I. Cooper, *J. Am. Chem. Soc.*, 2019, **141**, 9063–9071.
199 B. P. MacLeod, F. G. L. Parlane, T. D. Morrissey, F. Häse, L. M. Roch, K. E. Dettelbach, R. Moreira, L. P. E. Yunker, M. B. Rooney, J. R. Deeth, V. Lai, G. J. Ng, H. Situ, R. H. Zhang, M. S. Elliott, T. H. Haley, D. J. Dvorak, A. Aspuru-Guzik, J. E. Hein and C. P. Berlinguette, *Sci. Adv.*, 2020, **6**, eaaz8867.
200 F. Strieth-Kalthoff, H. Hao, V. Rathore, J. Derasp, T. Gaudin, N. H. Angello, M. Seifrid, E. Trushina, M. Guy, J. Liu, X. Tang, M. Mamada, W. Wang, T. Tsagaantsooj, C. Lavigne, R. Pollice, T. C. Wu, K. Hotta, L. Bodo, S. Li, M. Haddadnia, A. Wołos, R. Roszak, C. T. Ser, C. Bozal-Ginesta, R. J. Hickman, J. Vestfrid, A. Aguilar-Granda, E. L. Klimareva, R. C. Sigerson, W. Hou, D. Gahler, S. Lach, A. Warzybok, O. Borodin, S. Rohrbach, B. Sanchez-Lengeling, C. Adachi, B. A. Grzybowski, L. Cronin, J. E. Hein, M. D. Burke and A. Aspuru-Guzik, *Science*, 2024, **384**, eadk9227.
201 S. Steiner, J. Wolf, S. Glatzel, A. Andreou, J. M. Granda, G. Keenan, T. Hinkley, G. Aragon-Camarasa, P. J. Kitson, D. Angelone and L. Cronin, *Science*, 2019, **363**, eaav2211.

